Coupling of Slack and $Na_V1.6$ sensitizes Slack to quinidine blockade and guides anti-seizure strategy development

Tian Yuan[1#], Yifan Wang[1#], Yuchen Jin[1#], Shuai Xu[1], Heng Zhang[4], Qian Chen[1], Na Li[1], Xinyue Ma[1], Huifang Song[1], Chao Peng[1], Hui Yang[1], Ze Geng[1], Jie Dong[1], Guifang Duan[1], Qi Sun[1], Yang Yang[2], Fan Yang[3,4] and Zhuo Huang[1,5*]

AFFILATIONS

[1]State Key Laboratory of Natural and Biomimetic Drugs, Department of Molecular and Cellular Pharmacology, School of Pharmaceutical Sciences, Peking University Health Science Center, Beijing, 100191, China;

[2]Department of Medicinal Chemistry and Molecular Pharmacology, College of Pharmacy, Purdue University, West Lafayette, IN 47907, USA;

[3]Department of Biophysics, Kidney Disease Center of the First Affiliated Hospital, Zhejiang University School of Medicine, Hangzhou, Zhejiang, 310058, China;

[4]NHC and CAMS Key Laboratory of Medical Neurobiology, MOE Frontier Science Center for Brain Research and Brain-Machine Integration, School of Brain Science and Brain Medicine, Zhejiang University, Hangzhou, Zhejiang, 310058, China;

[5]IDG/McGovern Institute for Brain Research, Peking University, Beijing, 100871, China.

# These authors contribute equally to this work

*Correspondence: huangz@hsc.pku.edu.cn (Z.H.)

KEYWORDS

Slack, Nav1.6, quinidine, KCNT1-related epilepsy

GRAPHICAL ABSTRACT

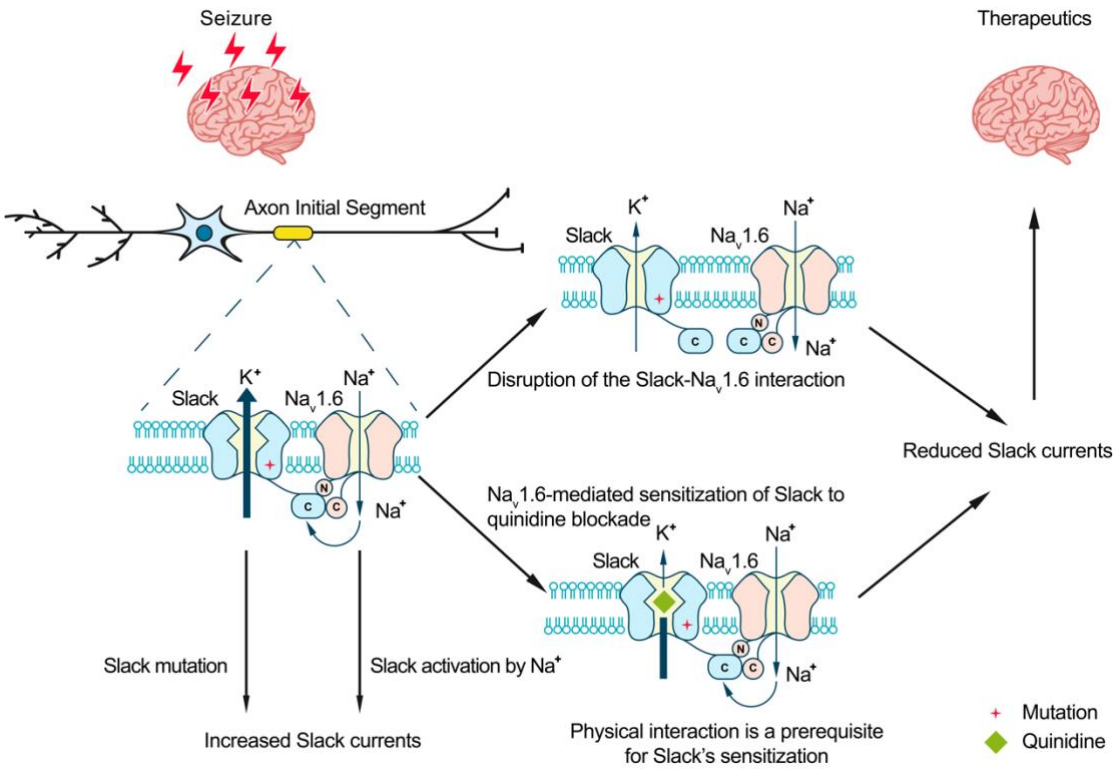

ABSTRACT

Quinidine has been used as an anticonvulsant to treat patients with KCNT1-related epilepsy by targeting gain-of-function KCNT1 pathogenic mutant variants. However, the detailed mechanism underlying quinidine's blockade against KCNT1 (Slack) remains elusive. Here, we report a functional and physical coupling of the voltage-gated sodium channel Nav1.6 and Slack. Nav1.6 binds to and highly sensitizes Slack to quinidine blockade. Homozygous knockout of Nav1.6 reduces the sensitivity of native sodium-activated potassium currents to quinidine blockade. Nav1.6-mediated

sensitization requires the involvement of $Na_V1.6$'s N- and C-termini binding to Slack's C-terminus, and is enhanced by transient sodium influx through $Na_V1.6$. Moreover, disrupting the Slack-$Na_V1.6$ interaction by viral expression of Slack's C-terminus can protect against $Slack^{G269S}$-induced seizures in mice. These insights about a Slack-$Na_V1.6$ complex challenge the traditional view of "Slack as an isolated target" for anti-epileptic drug discovery efforts, and can guide the development of innovative therapeutic strategies for KCNT1-related epilepsy.

INTRODUCTION

The sodium-activated potassium (K_{Na}) channels Slack and Slick were first identified in guinea pig cardiomyocytes, and were subsequently found to be encoded by two genes of the *Slo2* family[1,2]. Slack channels encoded by the *Slo2.2* (*KCNT1*) gene are gated by Na^+, while Slick channels encoded by the *Slo2.1* (*KCNT2*) gene are more sensitive to Cl^- than Na^+. Slack channels are expressed at high levels in the central nervous system (CNS), especially the cortex and brainstem[3-5]. Activation of Slack channels by intracellular sodium ions forms delayed outward currents in neurons, contributes to slow afterhyperpolarization (AHP) following repeated action potentials, and modulates the firing frequency of neurons[6,7].

Mutations in the *KCNT1* gene have been implicated in a wide spectrum of epileptic disorders, including early-onset epilepsy (*e.g.*, epilepsy of infancy with migrating focal seizures (EIMFS), non-EIMFS developmental and epileptic encephalopathies, and

autosomal dominant or sporadic sleep-related hypermotor epilepsy (ADSHE))[8-11]. Over 50 mutations related to seizure disorders have been identified, typically displaying a gain-of-function (GOF) phenotype in heterologous expression systems[11,12]. The prescribed antiarrhythmic drug, quinidine, has emerged as a precision therapy for KCNT1-related epilepsy by blocking Slack mutant variants *in vitro* and conferring decreased seizure frequency and improved psychomotor development in clinical treatment[13-16]. However, clinical quinidine therapy has shown limited success and contradictory therapeutic effects, probably due to poor blood–brain barrier penetration, dose-limiting off-target effects, phenotype-genotype associations, and rational therapeutic schedule[16-19].

Slack requires high intracellular free Na^+ concentrations ($[Na^+]_{in}$) for its activation in neurons (K_d of ~66 mM)[20]. However, previous investigations have shown that the $[Na^+]_{in}$ at resting states (~10 mM) is much lower than the $[Na^+]_{in}$ needed for effective Slack activation (*e.g.*, K_d value)[1,20,21]. Therefore, native Slack channels need to localize with Na^+ sources within a nanodomain to be activated and exert physiological function. Slack channels are known to be functionally coupled with sodium-permeable ion channels in neurons, such as voltage-gated sodium (Na_V) channels and AMPA receptors [21,22]. A question arises as to whether these known Na^+ sources modulate Slack's sensitivity to quinidine blockade.

Here, we found that $Na_V1.6$ sensitizes Slack to quinidine blockade. Slack and $Na_V1.6$ form a complex that functions in $Na_V1.6$-mediated transient sodium influx to sensitize

Slack to quinidine blockade in HEK293 cells and in primary cortical neurons. The widespread expression of these channel proteins in cerebral cortex, hippocampus, and cerebellum supports that the Nav1.6-Slack complex is essential for the function of a wide range of electrically excitable neurons, and moreover, that this complex can be viewed as a vulnerable target for drug development to treat KCNT1-related disorders.

RESULTS

Nav1.6 sensitizes Slack to quinidine blockade

Slack currents are activated by sodium entry through voltage-gated sodium (Nav) channels and ionotropic glutamate receptors (*e.g.* AMPA receptors)[21-23]. To investigate potential modulators of Slack's sensitivity to quinidine blockade, we initially focused on the known Na^+ sources of Slack. Working in HEK293 cells, we co-expressed Slack with AMPA receptor subunits (GluR1, GluR2, GluR3, or GluR4) or Nav channel α subunits (Nav1.1, Nav1.2, Nav1.3, or Nav1.6), which are highly expressed in the central nervous system[24-27]. The sensitivity of Slack to quinidine blockade was assessed based on the detected inhibitory effects of quinidine on delayed outward potassium currents[13,28]. Interestingly, all neuronal Nav channels significantly sensitized Slack to 30 μM quinidine blockade, whereas no effect was observed upon co-expression of Slack with GluR1, GluR2, GluR3, or GluR4 (Fig. S1).

When co-expressing Slack with Nav1.6 in HEK293 cells, Nav1.6 sensitized Slack to quinidine blockade by nearly 100-fold (IC_{50} = 85.13 μM for Slack expressed alone and

an IC_{50} = 0.87 μM for Slack upon co-expression with $Na_V1.6$) (Fig.1A,B,D,F). $Na_V1.6$ also exhibited >10-fold selectivity in sensitizing Slack to quinidine blockade against $Na_V1.1$, $Na_V1.2$, and $Na_V1.3$ (Fig. 1C,F, and Supplementary Table 1). When we co-expressed the cardiac sodium channel $Na_V1.5$ with Slack, we observed only ~3-fold sensitization of Slack to quinidine blockade (Fig.1E,F). These results together indicate that the apparent functional coupling between Slack and Na_V channels is Na_V-channel-subtype-specific, with $Na_V1.6$ being particularly impactful in Slack's responsivity to quinidine blockade.

Slack and Slick are both K_{Na} channels (with 74% sequence identity) and adopt similar structures[29], and Slick is also blocked by quinidine[30]. We next assessed whether $Na_V1.6$ sensitizes Slick to quinidine blockade and observed that, similar to Slack, co-expression of Slick and $Na_V1.6$ in HEK293 cells resulted in a sensitization of Slick to quinidine blockade (7-fold) (Fig. S2A,B). These results support that $Na_V1.6$ regulates both Slack and Slick and that $Na_V1.6$ can sensitize K_{Na} channels to quinidine blockade *in vitro*.

We also asked whether $Na_V1.6$ sensitizes native K_{Na} channels to quinidine blockade *in vivo*. We performed whole-cell patch-clamp recordings in primary cortical neurons from $Na_V1.6$-knockout C3HeB/FeJ mice and the wild-type littermate controls. K_{Na} currents (I_{KNa}) were isolated by replacing sodium ions with equivalent lithium ions in the bath solution (Fig. 1G,H). 3 μM quinidine significantly blocked native I_{KNa} (44%) in wild-type neurons (Fig. 1I,K), while the same concentration of quinidine had no significant effect on I_{KNa} in $Na_V1.6$-knockout ($Na_V1.6$-KO) neurons (Fig. 1J,K). These

results support that $Na_V1.6$ is required for the observed high sensitivity of native K_{Na} channels to quinidine blockade.

Transient sodium influx through $Na_V1.6$ enhances $Na_V1.6$-mediated sensitization of Slack to quinidine blockade

We next investigated the biomolecular mechanism underlying $Na_V1.6$-mediated sensitization of Slack to quinidine blockade. Considering that Slack currents are activated by sodium influx[22,29], we initially assessed the effects of $Na_V1.6$-mediated sodium influx on sensitizing Slack to quinidine blockade. We used 100 nM tetrodotoxin (TTX) to block $Na_V1.6$-mediated sodium influx (Fig. S3A,B)[31]. In HEK293 cells expressing Slack alone, 100 nM TTX did not affect Slack currents; nor did it affect Slack's sensitivity to quinidine blockade (IC_{50} = 83.27 μM) (Fig. 2A,B and Fig. S3C,D). In contrast, upon co-expression of Slack and $Na_V1.6$ in HEK293 cells, bath-application of 100nM TTX significantly reduced the effects of $Na_V1.6$ in sensitizing Slack to quinidine blockade (IC_{50} = 25.04 μM) (Fig. 2A,B). These findings support that sodium influx through $Na_V1.6$ contributes to $Na_V1.6$-mediated sensitization of Slack to quinidine blockade.

It is known that $Na_V1.6$-mediated sodium influx involves a transient inward flux that reaches a peak before subsequently decaying to the baseline within a few milliseconds; this is termed a transient sodium current (I_{NaT})[32]. A small fraction of $Na_V1.6$ currents are known to persist after the rapid decay of I_{NaT}, and these are termed persistent sodium currents (I_{NaP})[33]. We isolated I_{NaT} and I_{NaP} to explore their potential contributions in

sensitizing Slack to quinidine blockade. We selectively inactivated I_{NaT} using a depolarized prepulse of -40mV (Fig. S4A) and selectively blocked I_{NaP} by bath-application of 20 μM riluzole, which is a relatively specific I_{NaP} blocker that is known to stabilize inactivated-state Na_V channels and delay recovery from inactivation[34,35]. Our findings ultimately confirmed that the 20 μM riluzole selectively blocked I_{NaP} compared to I_{NaT} in HEK293 cells co-expressing Slack and $Na_V1.6$ (Fig. S4B) and that 20 μM riluzole had no effect on Slack currents when expressed alone (Fig. S4C,D).

Consistent with previous investigations[21,22], inactivating I_{NaT} reduced whole-cell Slack currents by 20%, and blocking I_{NaP} reduced Slack currents by 40% (Fig. 2C,D,F,G), supporting that $Na_V1.6$-mediated sodium influx activates Slack. Interestingly, inactivating I_{NaT} resulted in a > 20-fold decrease in Slack's sensitization to quinidine blockade (IC_{50} = 22.26 μM) (Fig. 2C,E). In contrast, blocking I_{NaP} had no effect on Slack's sensitization to quinidine blockade (IC_{50} = 1.60 μM) (Fig. 2F,H). These findings indicate that $Na_V1.6$ sensitizes Slack to quinidine blockade via I_{NaT} but not I_{NaP}.

Given that Slack current amplitudes are sensitive to sodium influx, and considering that quinidine is a sodium channel blocker, we examined whether $Na_V1.6$ has higher sensitivity to quinidine blockade than other Na_V channel subtypes, which could plausibly explain the observed increased strength of sensitization. We used whole-cell patch-clamping to assess the sensitivity of $Na_V1.1$, $Na_V1.2$, $Na_V1.3$, $Na_V1.5$, and $Na_V1.6$ to quinidine blockade. These sodium channels exhibited similar levels of quinidine

sensitivity (IC_{50} values in the range of 35.61-129.84 μM) (Fig. 2I,J and Supplementary Table 3), all of which were at least 40-fold lower than the $Na_V1.6$-mediated sensitization of Slack to quinidine blockade (Fig. 1F). Additionally, co-expressing Slack with $Na_V1.1$, $Na_V1.2$, $Na_V1.3$, $Na_V1.5$, or $Na_V1.6$ in HEK293 cells did not change the sensitivity of these Na_V channel subtypes to quinidine blockade (Fig. S5 and Supplementary Table 3). Thus, differential quinidine affinity for specific Na_V channel subtypes cannot explain the large observed $Na_V1.6$-mediated sensitization of Slack to quinidine blockade. Moreover, it is clear that $Na_V1.6$-mediated sensitization of Slack to quinidine blockade is directly mediated by I_{NaT}, rather than through some secondary effects related to $Na_V1.6$'s higher sensitivity to quinidine blockade.

Slack interacts with $Na_V1.6$ *in vitro* and *in vivo*

We found that the specific voltage-gated sodium channel blocker TTX did not completely abolish the effects of $Na_V1.6$ on sensitizing Slack to quinidine blockade (Fig. 2B), so it appears that a sodium-influx-independent mechanism is involved in the observed $Na_V1.6$-mediated sensitization of Slack to quinidine blockade. We therefore investigated a potential physical interaction between Slack and $Na_V1.6$. We initially assessed the cellular distribution of $Na_V1.2$, $Na_V1.6$, and Slack in the hippocampus and the neocortex of mouse. Consistent with previous studies[36,37], $Na_V1.2$ and $Na_V1.6$ were localized to the axonal initial segment (AIS) of neurons, evident as the co-localization of Na_V and AnkG, a sodium channel-associated protein known to accumulate at the AIS (Fig. 3A). Slack channels were also localized to the AIS of these neurons (Fig. 3A),

indicating that Slack channels are located in close proximity to $Na_V1.6$ channels, and supporting their possible interaction *in vivo*. Moreover, $Na_V1.6$ was co-immunoprecipitated with Slack in homogenates from mouse cortical and hippocampal tissues and from HEK293T cells co-transfected with Slack and $Na_V1.6$ (Fig. 3B,C), supporting that a physical interaction between Slack and $Na_V1.6$ occurs *in vivo*.

To assess the interaction between Slack and $Na_V1.6$ inside living cells, we performed a FRET assay in transfected HEK293T cells[38]. Briefly, we genetically fused mTFP1 and mVenus to the C-terminal regions of Slack and $Na_V1.6$, respectively (Fig. 3D). Upon imaging the emission spectra cells co-expressing $Na_V1.6$-mVenus and Slack-mTFP1 (measured at the plasma membrane region) (Fig. 3E), we detected positive FRET signals, indicating a Slack-$Na_V1.6$ interaction (Fig. 3F,H). The plasma membrane regions from HEK293T cells co-transfected with $Na_V1.6$ and Slack showed FRET efficiency values much larger than a negative control (in which standalone mVenus and mTFP1 proteins were co-expressed) (Fig. 3G,H), indicating that Slack channels reside in close spatial proximity (less than 10 nm) to $Na_V1.6$ channels in membranes of living cells.

We next characterized the consequences of the Slack-$Na_V1.6$ interaction in HEK293 cells using whole-cell recordings. Slack increased the rate of recovery from fast inactivation of $Na_V1.6$ (Fig. S6E), with no significant effects on the steady-state activation, steady-state fast inactivation, or ramp currents (Fig. S6C,D,F and Supplementary Table 3). Additionally, we found that $Na_V1.6$ had no significant effects

on the activation rate or the current-voltage (I-V) relationship of Slack currents (Fig. S6A,B). These results indicate that the physical interaction between Slack and $Na_V1.6$ produces functional consequences. Taken together, these findings support functional and physical coupling of Slack and $Na_V1.6$ *in vitro* and *in vivo*.

$Na_V1.6$'s N- and C-termini bind to Slack's C-terminus and sensitize Slack to quinidine blockade

To explore whether the physical interaction between Slack and $Na_V1.6$ is required for sodium-influx-mediated sensitization of Slack to quinidine blockade, we performed inside-out patch-clamp recordings on HEK293 cells transfected with Slack alone or co-transfected with Slack and $Na_V1.6$. Note that in these experiments the intracellular sodium concentration ($[Na^+]_{in}$) was raised to 140 mM (a concentration at which most Slack channels can be activated[20]), seeking to mimic the increased intracellular sodium concentration upon sodium influx. When expressing Slack alone, increasing the sodium concentration did not sensitize Slack to quinidine blockade (IC_{50} = 120.42 μM) (Fig. 4a). However, upon co-expression of $Na_V1.6$ and Slack, $Na_V1.6$ significantly sensitized Slack to quinidine blockade (IC_{50} = 2.91 μM) (Fig. 4A). These results support that physical interaction between Slack and $Na_V1.6$ is a prerequisite for sodium-influx-mediated sensitization of Slack to quinidine blockade.

To investigate which interacting domains mediate $Na_V1.6$'s sensitization of Slack to quinidine blockade, we focused on $Na_V1.6$'s cytoplasmic fragments, including its N-terminus, inter domain linkers, and C-terminus (Fig. 4B). Whole-cell recordings from

HEK293 cells co-expressing Slack with these $Na_V1.6$ fragments revealed that the N-terminus and C-terminus of $Na_V1.6$ significantly enhanced the sensitivity of Slack to quinidine blockade (IC_{50} = 31.59 μM for Slack upon co-expression with $Na_V1.6$'s N-terminus and IC_{50} = 43.70 μM for Slack upon co-expression with $Na_V1.6$'s C-terminus); note that the inter domain linkers had no effect (Fig. 4C).

Subsequent co-immunoprecipitation and glutathione S-transferase (GST) pull down assays of HEK293T cell lysates experimentally confirmed that $Na_V1.6$'s N- and C-termini each interact with Slack (Fig. 4D and Fig. S7). Additionally, whole-cell recordings using an $[Na^+]_{in}$ of 5 mM again showed that $Na_V1.6$'s N-terminus and $Na_V1.6$'s C-terminus sensitize Slack to quinidine blockade (IC_{50} = 27.87 μM) (Fig. 4E). And inside-out recordings using an $[Na^+]_{in}$ of 140 mM showed that co-expression of Slack, $Na_V1.6$'s N-terminus, and $Na_V1.6$'s C-terminus resulted in obvious sensitization of Slack to quinidine blockade, with an IC_{50} of 2.57 μM (Fig. 4F)—thus fully mimicking the aforementioned effects of full-length $Na_V1.6$ (IC_{50} = 2.91 μM) (Fig. 4A). These findings support that the binding of $Na_V1.6$'s N- and C-termini to Slack is required for $Na_V1.6$'s sensitization of Slack to quinidine blockade.

Recalling that $Na_V1.5$ had the least pronounced effect in sensitizing Slack to quinidine blockade among all examined Na_V channels (IC_{50} = 29.46 μM) (Fig. 1F and Supplementary Table 1). We constructed $Na_V1.5$-1.6 chimeras to test the roles of $Na_V1.6$'s N- and C-termini in sensitizing Slack to quinidine blockade. The replacement of both the N- and C-termini of $Na_V1.5$ with $Na_V1.6$'s N- and C-termini (namely

$Na_V1.5/6^{NC}$) fully mimicked effects of $Na_V1.6$ in sensitizing Slack to quinidine blockade (IC_{50} = 1.13 μM) (Fig. 4G-I). We also found that replacement of $Na_V1.5$'s N-terminus with $Na_V1.6$'s N-terminus (namely $Na_V1.5/6^{N}$) fully mimicked the effects of $Na_V1.6$ (IC_{50} = 1.18 μM) (Fig. 4G-I). Consistently, $Na_V1.5$'s C-terminus sensitized Slack to quinidine blockade (IC_{50} = 37.59 μM), whereas $Na_V1.5$'s N-terminus had no effect on Slack sensitization (Fig. 4C). These findings support that $Na_V1.6$'s N-terminus is essential for sensitizing Slack to quinidine blockade.

Having demonstrated that $Na_V1.6$ sensitizes Slack via $Na_V1.6$'s cytoplasmic N- and C-termini, we investigated which domains of Slack interact with $Na_V1.6$ and focused on Slack's cytoplasmic fragments, including Slack's N-terminus and C-terminus (Fig. 5A). In HEK293 cells co-expressing Na_V and Slack, Na_V-mediated sensitization of Slack to quinidine blockade was significantly attenuated upon the additional expression of Slack's C-terminus, but not of Slack's N-terminus (Fig. 5B,C), suggesting that Slack's C-terminus can disrupt the Slack-$Na_V1.6$ interaction by competing with Slack for binding to $Na_V1.6$. Consistently, Slack's C-terminus co-immunoprecipitated with $Na_V1.6$'s N- and C-termini in HEK293T cell lysates (Fig. 5D). Together, these results support that Slack's C-terminus physically interacts with $Na_V1.6$ and that this interaction is required for $Na_V1.6$'s sensitization of Slack to quinidine blockade.

$Na_V1.6$ binds to and sensitizes epilepsy-related Slack mutant variants to quinidine blockade

Over 50 mutations in KCNT1 (Slack) have been identified to related to seizure disorders[11]. Having established that $Na_V1.6$ can sensitize wild-type Slack to quinidine blockade, we next investigated whether $Na_V1.6$ also sensitizes epilepsy-related Slack mutant variants to quinidine blockade. We chose 3 Slack pathogenic mutant variants (K629N, R950Q, and K985N) initially detected in patients with KCNT1-related epilepsy[15,39,40]. Considering that these 3 mutations are located in Slack's C-terminus, and recalling that Slack's C-terminus interacts with $Na_V1.6$ (Fig. 5D), we first used co-immunoprecipitation assays and successfully confirmed that each of these Slack mutant variants interacts with $Na_V1.6$ in HEK293T cell lysates (Fig. 6A).

Subsequently, whole-cell recordings revealed that $Na_V1.6$ significantly sensitized all of the examined Slack mutant variants to quinidine blockade, with IC_{50} values ranging from 0.26 to 2.41 μM (Fig. 6B-D and Supplementary Table 4). These results support that $Na_V1.6$ interacts with examined Slack mutant variants and sensitizes them to quinidine blockade. It is plausible that the Slack-$Na_V1.6$ interaction contributes to the therapeutical role of quinidine in the treatment of KCNT1-related epilepsy.

Viral expression of Slack's C-terminus prevents Slack^{G269S}-induced seizures

Having established that blocking $Na_V1.6$-mediated sodium influx significantly reduced Slack current amplitudes (Fig. 2D,G), we found that the heterozygous knockout of $Na_V1.6$ significantly reduced the afterhyperpolarization amplitude in murine hippocampal neurons (Fig. S8), together indicating that $Na_V1.6$ activates native Slack through providing Na^+. We therefore assumed that disruption of the Slack-$Na_V1.6$

interaction should reduce the amount of Na^+ in the close vicinity of epilepsy-related Slack mutant variants and thereby counter the increased current amplitudes of these Slack mutant variants. Pursuing this, we disrupted the Slack-Na_V interaction by overexpressing Slack's C-terminus (to compete with Slack) and measured whole-cell current densities. In HEK293 cells co-expressing epilepsy-related Slack mutant variants (G288S, R398Q)[41,42] and Na_V, expression of Slack's C-terminus significantly reduced whole-cell current densities of $Slack^{G269S}$ and $Slack^{R398Q}$ (Fig. 7A,B), supporting that disrupting the Slack-Na_V1.6 interaction can indeed reduce current amplitudes of Slack mutant variants, which may protect against seizures induced by Slack mutant variants.

We next induced an *in vivo* epilepsy model by introducing a Slack G269S variant into C57BL/6N mice using adeno-associated virus (AAV) injection to mimic the human Slack mutation G288S[41]. Specifically, we delivered stereotactic injections of AAV9 containing expression cassettes for $Slack^{G269S}$ (or GFP negative controls) into the hippocampal CA1 region of 3-week-old C57BL/6N mice (Fig. 7C,D). At 3-5 week intervals after AAV injection, we quantified the seizure susceptibility of mice upon the induction of a classic kainic acid (KA) model of temporal lobe epilepsy[43,44]. In this model, seizures with stage IV or higher (as defined by a modified Racine, Pinal, and Rovner scale[45]) are induced in rodents by intraperitoneal administration of 28 mg/kg KA.

We assessed a time course of KA-induced seizure stages at 10-min intervals and found that viral expression of $Slack^{G269S}$ resulted in faster seizure progression in mice

compared to control GFP expression (Fig. 7E). We calculated the total seizure score per mouse to assess seizure severity[46]. Slack^{G269S}-expressing mice showed significantly higher seizure severity than GFP-expressing mice (Fig. 7F). The percentage of mice with stage VI~IX seizures also increased, from 9.1% in GFP-expressing control mice to 58.3% in the Slack^{G269S}-expressing mice (Fig. 7G). These results support that viral expression of Slack^{G269S} significantly increases seizure susceptibility in mice.

To evaluate the potential therapeutic effects of disrupting the Slack-Nav1.6 interaction, we delivered two AAV9s (one for Slack^{G269S} and one for Slack's C-terminus [residues 326-1238]) into the CA1 region of mice (Fig. 7D). Viral expression of Slack's C-terminus in Slack^{G269S}-expressing mice significantly decreased seizure progression, seizure severity, and the percentage of mice experiencing stage VI~IX seizures (Fig. 7E-G). These results support that viral expression of Slack's C-terminus can prevent Slack^{G269S}-induced seizures in mice, thus showcasing that using Slack's C-terminus to disrupt the Slack-Nav1.6 interaction is a promising therapeutic intervention to treat KCNT1-related epilepsy.

DISCUSSION

We here found that Nav1.6's N- and C- termini bind to Slack's C-terminus and sensitize Slack to quinidine blockade via Nav1.6-mediated transient sodium currents. These results suggest that the pharmacological blocking effects of a channel blocker are not exclusively mediated by the channel *per.se*., but modulated by channel's interacting

proteins. Moreover, we show that viral expression of Slack's C-terminus can rescue the increased seizure susceptibility and confer protection against Slack^{G269S}-induced seizures in mice.

At resting membrane potential, the intracellular sodium concentration ($[Na^+]_{in}$) in neurons (equal to ~10 mM) is too low to effectively activate Slack (K_d of 66 mM)[1,20]. Slack is functionally coupled to sodium influx, which is known to be mediated by ion channels and receptors, including Nav, AMPARs, and NMDARs[21-23,47]. Such Na^+ sources can provide both the membrane depolarization and the Na^+ entry known to be required for Slack activation, enabling Slack to contribute both to action potential repolarization during neuronal high-frequency firing[7,48] and to regulating excitatory postsynaptic potential (EPSP) at post-synaptic neurons[23]. Our results support that Slack and Nav1.6 form a channel complex, while also implying that Nav1.6-mediated sodium influx increases the Na^+ concentration in the close vicinity of Slack to activate Slack. As a low threshold Nav channel subtype, Nav1.6 has been reported to dominate the initiation and propagation of action potentials in axon initial segments (AIS) in excitatory neurons[36,49-51]. The activation of Slack by Nav1.6 at AIS has multiple impacts, including ensuring the timing of the fast-activated component of Slack currents, regulating the action potential amplitude, and apparently contributing to intrinsic neuronal excitability[29].

An interesting question arises from our observation that Slack's sensitivity to quinidine blockade is enhanced by I_{NaT} but not I_{NaP}: what can explain the distinct I_{NaT} and I_{NaP}

contributions? We speculate that with physical modulation by $Na_V1.6$, I_{NaT} may elicit a specific open conformation of Slack that brings its quinidine binding pocket into a high affinity state, which could lead to a substantial increase in Slack's sensitivity to quinidine blockade. The possibility of this hypothetical open conformation is supported by previous reports of the presence of subconductance states detected in single-channel recordings of *Xenopus* oocytes expressing Slack channels[52], which implies that there are multiple open conformations of Slack. Although only one open conformation of Slack has been observed in cryo-EM, the gap between maximum conformational open probability (~1.0) and maximum functional open probability (~0.7) implies a subclass within this class of open channels[53].

As previously mentioned, gain-of-function Slack mutant variants have been linked to a broad spectrum of epileptic disorders that are accompanied by intellectual disabilities and both psychomotor and developmental defects[18,54]. Given that many patients are refractory or non-responsive to conventional anticonvulsants[12,54,55], and considering the limited success of quinidine in clinical treatment of KCNT1-related epilepsy, inhibitors targeting Slack are needed urgently[18]. Several small-molecule inhibitors against Slack have been reported, providing informative starting points for drug development efforts with KCNT1-related epilepsy[28,56,57]. However, our discovery of the Slack-$Na_V1.6$ complex challenges the traditional view that Slack acts as an isolated target in KCNT1-related epilepsy[18]. Indeed, our study supports that co-expression of Slack and $Na_V1.6$ in heterologous cell models should be performed when analyzing clinically relevant

Slack mutations and when screening anti-epileptic drugs for use in treating KCNT1-related disorders.

Genotype-phenotype analysis has shown that ADSHE-related mutations are clustered in the regulator of conductance of K^+ (RCK2) domain; while EIMFS-related mutations do not show a particular pattern of distribution[11]. All functionally tested Slack mutant variants show gain-of-function phenotypes, with increased Slack currents [9,11,18]. Further, the epilepsy-related Slack mutant variants confer their gain-of-function phenotypes through two molecular mechanisms: increasing maximal channel open probability (P_{max}) or increasing sodium sensitivity (K_d) of Slack[58]. Both P_{max} and K_d are highly sensitive to $[Na^+]_{in}$; these are respectively analogous to the efficacy and potency of $[Na^+]_{in}$ on Slack currents[58]. Notably, several Slack mutant variants show gain-of-function phenotypes only at high $[Na^+]_{in}$ (*e.g.* 80 mM)[58]. These results indicate that the gain-of-function phenotype of epilepsy-related Slack mutant variants is aggravated by high $[Na^+]_{in}$. Our discovery of functional coupling between $Na_V1.6$ and Slack presents a plausible basis for how $Na_V1.6$-mediated sodium influx can increase $[Na^+]_{in}$ and thus apparently aggravate the gain-of-function phenotype of Slack mutant variants. Therefore, it makes sense that disruption of the Slack-$Na_V1.6$ interaction by overexpressing Slack's C-terminus reduces the current amplitudes of gain-of-function Slack mutant variants (Fig. 7A,B). Our successful demonstration that viral expression of Slack's C-terminus prevents epilepsy-related $Slack^{G269S}$-induced seizures in mice

(Fig. 7E-G) warrants further translational evaluation for developing therapeutic interventions to treat KCNT1-related epilepsy.

METHODS

Animals

C57BL/6 mice were purchased from Charles River Laboratories. $Na_V1.6$ knockout C3HeB/FeJ mice were generous gifts from Professor Yousheng Shu at Fudan University. All animals were housed on a 12-hour light/dark cycle with *ad libitum* access to food and water. All procedures related to animal care and treatment were approved by the Peking University Institutional Animal Care and Use Committee and met the guidelines of the National Institute of Health Guide for the Care and Use of Laboratory Animals. Each effort was made to minimize animal suffering and the number of animals used. The experiments were blind to viral treatment condition during behavioral testing.

Antibodies and Reagents

Commercial antibodies used were: anti-AnkG (Santa Cruz), anti-Slack (NeuroMab), anti-$Na_V1.2$ (Alomone), anti-$Na_V1.6$ (Alomone), anti-HA (Abbkine), anti-Flag (Abbkine), anti-β-Actin (Biodragon), HRP Goat Anti-Mouse IgG LCS (Abbkine), HRP Mouse Anti-Rabbit IgG LCS (Abbkine), Alexa Fluor 488-AffinityPure Fab Fragment Donkey anti-rabbit IgG (Jackson), Alexa Fluor 594 Donkey anti-mouse IgG (Yeason). GPCR Extraction Reagent was from Pierce, NP40 lysis buffer was from Beyotime,

protease inhibitor mixture cocktail was from Roche Applied Science, rabbit IgG and mouse IgG was from Santa Cruz, and Protein G Dynabeads were from Invitrogen. Tetrodotoxin was from Absin Bioscience. Quinidine was from Macklin, and riluzole was from Meilunbio. All other reagents were purchased from Sigma-Aldrich.

Molecular cloning

Human Slack-B (Ref Seq: NM_ 020822.3) and $Na_V1.6$ (Ref Seq: NM_ 014191.4) were subcloned into the modified pcDNA3.1(+) vector using Gibson assembly. All mutations and chimeras of ion channels were also constructed using Gibson assembly. For GST pull down assay, the segments of Slack and $Na_V1.6$ were subcloned into pCDNA3.1(+) and pGEX-4T-1 vector, respectively. For FRET experiments, mVenus-tag was fused to the C-terminus of $Na_V1.6$ sequence, and mTFP1-tag was also fused to the C-terminus of Slack sequence.

Immunoprecipitation

The brain tissues or HEK293T cells co-expressing full-length or fragments of Slack and $Na_V1.6$ were homogenized and lysed in GPCR Extraction Reagent (Pierce) with cocktail for 30 min at 4 °C. The homogenate was centrifuged for 20 min at 16 000 g and 4 °C to remove cell debris and then supernatant was incubated with 5 μg Slack antibody (NeuroMab) or Nav1.6 antibody (Alomone) for 12 h at 4 °C with constant rotation. 40 μl of protein G Dynabeads (Invitrogen) was then added and the incubation was continued until the next day. Beads were then washed three times with NP40 lysis.

Between washes, the beads were collected by DynaMag. The remaining proteins were eluted from the beads by re-suspending the beads in 1×SDS-PAGE loading buffer and incubating for 30 min at 37 °C. The resultant materials from immunoprecipitation or lysates were then subjected to western blot analysis.

Western blot analysis

Proteins suspended in 1×SDS-PAGE loading buffer were denatured for 30 min at 37 °C. Then proteins were loaded on 6% or 8% sodium dodecyl sulphate–polyacrylamide gel electrophoresis and transferred onto nitrocellulose filter membrane (PALL). Non-specific binding sites were blocked with Tris-buffered saline-Tween (0.02 M Tris, 0.137 M NaCl and 0.1% Tween 20) containing 5% non-fat dried milk. Subsequently, proteins of interest were probed with primary antibodies for overnight at 4 °C. After incubation with a secondary antibody, immunoreactive bands were visualized using HRP Substrate Peroxide Solution (Millipore) according to the manufacturer's recommendation.

GST pull down assay

Plasmids encoding GST-fused $Na_V1.6$ segments were transformed into BL21(DE3). After expressing recombinant proteins induced by overnight application of isopropyl-1-thio-β-D-galactopyranoside (IPTG) (0.1mM) at 25°C, the bacteria were collected, lysed and incubated with GSH beads using BeaverBeads GSH kit (Beaver) according to the manufacturer's instruction.

Plasmids encoding KCNT1 channel or HA-tagged KCNT1 segments were transfected into HEK293T cells using lipofectamine 2000 (Introvigen). 40 h after transfection, cells were lysed in NP40 lysis buffer with inhibitor cocktail, and then centrifugated at 4 ℃, 15000 g for 20 min. The supernatants were incubated with protein-bound beads. The protein-bound beads were washed by washing buffer (50 mM Tris-HCl pH = 7.4, 120 mM NaCl, 2 mM EGTA, 2 mM DTT, 0.1% triton X-100, and 0.2% Tween-20) for 5 min 3 times and then denatured with 1×SDS-PAGE loading buffer and incubating for 30 min at 37 °C. The resultant materials were subjected to western blot analysis.

Cell culture

The human embryonic kidney cells (HEK293 and HEK293T) were maintained in Dulbecco's Modified Eagle Medium (DMEM, Gibco) supplemented with 15% Fetal Bovine Serum (FBS, PAN-Biotech) at 37ºC and 5% CO_2. Primary cortical neurons were prepared from either sex of postnatal homozygous $Na_V1.6$ knockout C3HeB/FeJ mice and the wild-type littermate controls. After the mice were decapitated, the cortices were removed and separated from the meninges and surrounding tissue. Tissues were digested in 2 mg/mL Papain (Aladdin) containing 2 μg/mL DNase I (Psaitong) for 30 min followed by centrifugation and resuspension. Subsequently, the cells were plated on poly-D-lysine (0.05 mg/mL) pre-coated glass coverslips in plating medium (DMEM containing 15% FBS), at a density of 4×10^5 cells/ml, and cultivated at 37°C and 5% CO_2 in a humidified incubator. 5 h after plating, the medium was replaced with Neurobasal Plus medium (Invitrogen) containing 2% v/v B-27 supplement (Invitrogen),

2 mM Glutamax (Invitrogen), 50 U/mL penicillin and streptomycin (Life Technologies). The primary neurons were grown 6-10 days before electrophysiological recordings with half of the media replaced every three days.

Voltage-clamp recordings

The plasmids expressing full-length or fragments of Slack and Na_V channels (excluding full-length $Na_V1.6$) were co-transfected into HEK293 cells using lipofectamine 2000 (Introvigen). To co-express Slack with $Na_V1.6$, the plasmid expressing Slack was transfected into a stable HEK293 cell line expressing $Na_V1.6$. 18-36 h after transfection, voltage-clamp recordings were obtained using a HEKA EPC-10 patch-clamp amplifier (HEKA Electronic) and PatchMaster software (HEKA Electronic). For all whole-cell patch clamp experiments in HEK cells except for data presented in Fig. S2d, the extracellular recording solution contained (in mM): 140 NaCl, 3 KCl, 1 $CaCl_2$, 1 MgCl2, 5 glucose, 10 HEPES, 1 Tetraethylammonium chloride (310 mOsm/L, pH 7.30 with NaOH). The recording pipette intracellular solution (5 mM Na) contained (in mM): 100 K-gluconate, 30 KCl, 15 Choline-Cl, 5 NaCl, 10 glucose,5 EGTA, 10 HEPES (300 mOsm/L, pH 7.30 with KOH). For data presented in Fig. S2d, the extracellular recording solution remains the same as above, the pipette intracellular solution contained (in mM): 140 CsF, 10 NaCl, 5 EGTA, 10 HEPES (pH 7.30 with NaOH), indicating that the unusual right shifts (15~20 mV) in voltage dependence of $Na_V1.6$ were induced by components in pipette solution, not recording system errors. For primary cortical neurons, intracellular solution (0 mM Na) was used to prevent the

activation of sodium-activated potassium channels by basal intracellular sodium ions. NaCl in the intracellular solution was replaced with choline chloride in an equimolar concentration. For inside out patch-clamps, the bath solution contained (in mM): 140 NaCl, 1 EDTA, 10 HEPES and 2 $MgCl_2$ (310 mOsm/L, pH 7.30 with NaOH). Pipette solution contained (in mM): 130 KCl, 1 EDTA, 10 HEPES and 2 $MgCl_2$ (300 mOsm/L, pH 7.30 with KOH). The pipettes were fabricated by a DMZ Universal Electrode puller (Zeitz Instruments) using borosilicate glass, with a resistance of 1.5-3.5 MΩ for whole-cell patch clamp recordings and 8.0-10.0 MΩ for inside-out patch clamp recordings. All experiments were performed at room temperature. The concentration-response curves were fitted to four-parameter Hill equation:

$$Y = Bottom + (Top - Bottom)/(1 + 10^{X - lgIC_{50}}) \qquad (1)$$

where Y is the value of $I_{Quinidine}/I_{Control}$, Top is the maximum response, Bottom is the minimum response, X is the lg of concentration, and IC_{50} is the drug concentration producing the half-maximum response. Significance of fitted IC_{50} values compared to control was analyzed using extra sum-of-squares F test.

For data presented in fig. S3, cells were excluded from analysis if series resistance > 5 MΩ and series resistance compensation was set to 70%~90%.

The time constants (τ) of activation were fitted with a single exponential equation:

$$I(t) = Offset + A * exp(-\frac{t}{\tau}) \qquad (2)$$

where I is the current amplitude, t is time, offset represents the asymptote of the fit, and A represents the amplitude for the activation or inactivation.

Steady-state fast inactivation (I-V) and conductance-voltage (G-V) relationships were fitting with Boltzmann equations:

$$I/I_{max} = 1/(1 + \exp\left(\frac{V_m - V_{1/2}}{k}\right)) \qquad (3)$$

$$G/G_{max} = 1/(1 + \exp\left(\frac{V_m - V_{1/2}}{k}\right)) \qquad (4)$$

$$G = I/(V_m - E_{Na}) \qquad (5)$$

where I is the peak current, G is conductance, V_m is the stimulus potential, $V_{1/2}$ is the midpoint voltage, E_{Na} is the equilibrium potential, and k is the slope factor. Significance of fitted $V_{1/2}$ compared to control was analyzed using extra sum-of-squares F test.

Recovery from fast inactivation data were fitted with a single exponential equation:

$$I/I_{max} = A * (1 - exp\left(-\frac{t}{\tau}\right)) \qquad (6)$$

Where I is the peak current of test pulse, I_{max} is the peak current of first pulse, A is the proportional coefficient, t is the delay time between the two pulses, and τ is the time constant of recovery from fast inactivation.

Acute slice preparation and current-clamp recordings

Horizontal slices containing hippocampus were obtained from 6-8 weeks old heterozygous $Na_V1.6$ knockout ($Scn8a^{+/-}$) C3HeB/FeJ mice and the wild-type littermate controls. In brief, animals were anesthetized and perfused intracardially with ice-cold

modified “cutting solution” containing (in mM): 110 choline chloride, 2.5 KCl, 0.5 $CaCl_2$, 7 $MgCl_2$, 25 $NaHCO_3$, 1.25 NaH_2PO_4, 10 glucose; bubbled continuously with 95%O_2/5%CO_2 to maintain PH at 7.2. The brain was then removed and submerged in ice-cold “cutting solution”. Next, the brain was cut into 300 μm slices with a vibratome (WPI). Slices were incubated in oxygenated (95% O_2 and 5% CO_2) “recording solution” containing (in mM): 125 NaCl, 2.5 KCl, 2 $CaCl_2$, 2 $MgCl_2$, 25 $NaHCO_3$, 1.25 NaH_2PO_4, 10 glucose (315 mOsm/L, PH 7.4, 37°C) for 30 min, and stored at room temperature.

Slices were subsequently transferred to a submerged chamber containing “recording solution” maintained at 34-36 °C. Whole-cell recordings were obtained from hippocampal CA1 neurons under a ×60 water-immersion objective of an Olympus BX51WI microscope (Olympus). Pipettes had resistances of 5-8 MΩ. For current-clamp recordings, the external solution (unless otherwise noted) was supplemented with 0.05 mM (2R)-amino-5-phosphonovaleric acid (APV), 0.01 mM 6-cyano-7-nitro-quinoxaline-2,3-dione, 0.01 mM bicuculline and 0.001 mM CGP 55845, and internal pipette solution containing (in mM): 118 $KMeSO_4$, 15 KCl, 10 HEPES, 2 $MgCl_2$, 0.2 EGTA, and 4 Na_2ATP, 0.3 Tris-GTP, 14 Tris-phosphocreatinin (pH 7.3 with KOH).

In our whole-cell current-clamp recordings with an Axon 700B amplifier (Molecular Devices), we initially applied a 100 ms, 20 pA test pulse to the recording neurons right after breaking into the whole-cell configuration. A fast-rising component and a slow-rising component of voltage response were clearly visible. Then we zoomed into the fast-rising component of the voltage responses and turned up the pipette capacitance

neutralization slowly to shorten the rise time of the fast-rising component until the oscillations of voltage responses appeared. Subsequently, we decreased the capacitance compensation just until the oscillations disappeared. For bridge balance of current-clamp recordings, we increased the value of bridge balance slowly until the fast component of the voltage response disappeared, and the slow-rising component appeared to rise directly from the baseline. Series resistance and pipette capacitance were compensated using the bridge balance and pipette capacitance neutralization options in the Multiclamp 700B command software (Molecular Devices). The bridge balance value was between 20 and 30 MΩ and the pipette capacitance neutralization value was between 3 and 5 pF. For in vitro experiments, the cells were selected by criteria based on hippocampal CA1 cell morphology and electrophysiological properties in the slices. Electrophysiological recordings were made using a Multiclamp 700B amplifier (Molecular Devices). Recordings were filtered at 10 kHz and sampled at 50 kHz. Data were acquired and analyzed using pClamp10.0 (Molecular Devices). Series resistance was in the order of 10–30 MΩ and was approximately 60–80% compensated. Recordings were discarded if the series resistance increased by more than 20% during the time course of the recordings.

Fluorescence Imaging and FRET Quantification

The spectroscopic imaging was built upon a Nikon TE2000-U microscope. The excitation light was generated by an Ar laser. The fluorescent protein mVenus fused to $Na_V1.6$ and mTFP1 fused to Slack were excited by laser line at 500 and 400-440 nm,

respectively. The duration of light exposure was controlled by a computer-driven mechanical shutter (Uniblitz). A spectrograph (Acton SpectraPro 2150i) was used in conjunction with a charge coupled device (CCD) camera (Roper Cascade 128B). In this recording mode two filter cubes (Chroma) were used to collect spectroscopic images from each cell (excitation, dichroic): cube I, D436/20, 455dclp; cube II, HQ500/20, Q515lp. No emission filter was used in these cubes. Under the experimental conditions, auto fluorescence from untransfected cells was negligible. Fluorescence imaging and analysis were done using the MetaMorph software (Universal Imaging). User-designed macros were used for automatic collection of the bright field cell image, the fluorescence cell image, and the spectroscopic image. Emission spectra were collected from the plasma membrane of the cell by positioning the spectrograph slit across a cell and recording the fluorescence intensity at the position corresponding to the membrane region (Fig. 2e, dotted lines in red); the same slit position applied to both the spectrum taken with the mTFP1 excitation and the spectrum taken with the mVenus excitation. Using this approach, the spectral and positional information are well preserved, thus allowing reliable quantification of FRET efficiency specifically from the cell membrane. Spectra were corrected for background light, which was estimated from the blank region of the same image.

FRET data was quantified in two ways. First, the FRET ratio was calculated from the increase in mVenus emission due to energy transfer as described in the previous study.[59] Briefly, mTFP1 emission was separated from mVenus emission by fitting of standard

spectra acquired from cells expressiring only mVenus or mTFP1. The fraction of mVenus-tagged molecules that are associated with mTFP1-tagged molecules, Ab, is calculated as

$$Ab = 1/(1 + K_D/[\text{Dfree}]) \qquad (7)$$

where K_D is the dissociation constant and [Dfree] is the concentration of free donor molecules. Note that

$$FRET\ Ratio = 1 + Ab * (FRET\ Ratio_{max} - 1) \qquad (8)$$

Regression analysis was used to estimate Ab in individual cells. From each cell, the FRET ratio_{exp} was experimentally determined. The predicted Ab value was then computed by adjusting two parameters, FRET Ratio_{max} and apparent K_D. Ab was in turn used to give a predicted FRET ratiopredicted. By minimizing the squared errors (FRET ratio_{exp} – FRET $\text{ratio}_{predicted})^2$, K_D was determined.

Second, apparent FRET efficiency was also calculated from the enhancement of mVenus fluorescence emission due to energy transfer[59-62] using a method as previously described.[63] Briefly, Ratio A_0 and Ratio A were measured to calculate FRET efficiency. Ratio A_0 represents the ratio between tetramethylrhodamine maleimide emission intensities (in the absence of fluorescein maleimide) upon excitation at the donor and acceptor excitation wavelengths[62-64], and was calculated in the present study at the mVenus peak emission wavelength. A particular advantage of quantifying Ratio A_0 for FRET measurement is that changes in fluorescence intensity caused by many

experimental factors can be cancelled out by the ratiometric measurement. A similar ratio, termed Ratio A, was determined in the presence of mTFP1 in the same way as Ratio A_0. If FRET occurred, the Ratio A value should be higher than Ratio A_0; the difference between Ratio A and Ratio A_0 was directly proportional to the FRET efficiency by the factor of extinction coefficient ratio of mTFP1 and mVenus.[62-64]

Immunostaining

After deep anesthesia with sodium pentobarbital, mice were sacrificed by perfusion with 0.5% paraformaldehyde and 0.5% sucrose (wt/vol) in 0.1 M phosphate buffer (pH 7.4). The brain was removed and post-fixed in the same fixative for 2 h, and subsequently immersed in 30% sucrose in 0.1 M phosphate buffer for 48 h. Cryostat coronal sections (20 μm) were obtained using a freezing microtome (Leica). The sections were rinsed in 0.01 M phosphate-buffered saline (PBS, pH 7.4), permeabilized in 0.5% Triton X-100 in PBS for 30 min, and incubated in a blocking solution (5% BSA, 0.1% Triton X-100 in PBS, vol/vol) at 20–25 °C for 2 h, followed by overnight incubation at 4 °C with primary antibody to AnkG (1:100, Santa Cruz, sc-31778), Slack (1:100, NeuroMab, 73-051), $Na_V1.2$ (1:200, Alomone, ASC-002), $Na_V1.6$ (1:200, Alomone, ASC-006), Flag (1:500, Abbkine, ABT2010), and HA (1:500, Abbkine, ABT2040) in blocking solution. After a complete wash in PBS, the sections were incubated in Alexa 488-conjugated doney anti-rabbit IgG and Alexa 594 donkey anti-mouse IgG in blocking solution at 20–25 °C for 2 h. The sections were subsequently washed and rinsed in Dapi solution. Images were taken in the linear range of the

photomultiplier with a laser scanning confocal microscope (ZEISS LSM 510 META NLO).

Adeno-associated virus construction and injection

The adeno-associated viruses (AAVs) and the negative GFP control were from Shanghai GeneChem. Co., Ltd. The full-length $Slack_{G269S}$ sequence (1-1238aa) was ligated into modified CV232 (CAG-MCS-HA-Poly A) adeno-associated viral vector. The Slack's C-terminus sequence (326-1238aa) and the negative control were ligated into GV634 (CAG-MCS-3×Flag-T2A-EGFP-SV40-Poly A) adeno-associated viral vector. The viruses (>10^{11} TU/ml) were used in the present study.

For dorsal CA1 viral injection, C57BL/6J mice aged 3 weeks were anesthetized with isoflurane and placed in a stereotaxic apparatus (RWD Life Science Co., Ltd.). Using a 5 μL micro syringe (Hamilton) with a 30 gauge needle (RWD Life Science Co., Ltd.), 600 nL of the viruses was delivered at 10 nL/min by a micro-syringe pump (RWD Life Science Co., Ltd.) at the following site in each of the bilateral CA1 regions, using the stereotaxic coordinates: 2.5 mm (anterior-posterior) from bregma, 2 mm (medio-lateral), ± 1.5 mm (dorsal-ventral)[65]. The syringe was left in place for 5 min after each injection and withdrawn slowly. The exposed skin was closed by surgical sutures and returned to home cage for recovery. All the experiments were conducted after at least 3 weeks of recovery. All the mice were sacrificed after experiments to confirm the injection sites and the viral trans-infection effects by checking EGFP under a fluorescence microscope (ZEISS LSM 510 META NLO).

Kainic acid-induced status epilepticus

KA (Sigma-Aldrich) was intraperitoneally administered to produce seizures with stage IV or higher. The dose of kainite acid used was 28 mg/kg for mice (6–8 weeks)[66,67]. To assess epilepsy susceptibility, seizures were rated using a modified Racine, Pinal, and Rovner scale[45,68]: (1) Facial movements; (2) head nodding; (3) forelimb clonus; (4) dorsal extension (rearing); (5) Loss of balance and falling; (6) Repeated rearing and failing; (7) Violent jumping and running; (8) Stage 7 with periods of tonus; (9) Dead. Seizures was terminated 2 h after onset with the use of sodium pentobarbital (30 mg/kg; Sigma-Aldrich).

Statistical analysis

For in vitro experiments, the cells were evenly suspended and then randomly distributed in each well tested. For in vivo experiments, the animals were distributed into various treatment groups randomly. Statistical analyses were performed using GraphPad Prism 9 (GraphPad Software) and SPSS 26.0 software (SPSS Inc.). Before statistical analysis, variation within each group of data and the assumptions of the tests were checked. Comparisons between two independent groups were made using unpaired Student's two-tailed t test. Comparisons among nonlinear fitted values were made using extra sum-of-squares F test. Comparisons among three or more groups were made using one- or two-way analysis of variance followed by Bonferroni's post hoc test. No statistical methods were used to predetermine sample sizes but our sample sizes are similar to those reported previously in the field[37,69]. All experiments and analysis of data were

performed in a blinded manner by investigators who were unaware of the genotype or manipulation. * $p < 0.05$, ** $p < 0.01$, *** $p < 0.001$, **** $p < 0.0001$. All data are presented as mean ± SEM.

AUTHOR CONTRIBUTIONS

T.Y. and Y.J. performed and analyzed voltage-clamp recordings. Y.W. performed and analyzed Western blotting, immunoprecipitation. S.X., C.P., and G.D. performed and analyzed pull down assay. Q.C. performed the immunostaining. H.Z. and F.Y. performed and analyzed the FRET imaging. H.S., N.L., and X.M. performed and analyzed the current clamp recordings. T.Y., H.Y., Z.G., and J.D. performed the molecular cloning. Z.H., T.Y., and Y.W. designed the experiments. Z.H., T.Y., and Y.J. wrote the manuscript. Z.H., F.Y., Y.Y., and Q.S. reviewed the manuscript.

ACKNOWLEDGMENTS

This work was supported by Chinese National Programs for Brain Science and Brain-like intelligence technology No.2021ZD0202102 to Z.H.; National Natural Science Foundation of China Grant (Nos. 31871083 and 81371432 to Z.H.; Nos. 32000674 to G.D.). We also thank Professor Yousheng Shu at Fudan University for providing the Nav1.6-knockout mice.

DATA AVAILABILITY

The data that support the findings of this study are available from the corresponding author upon reasonable request.

REFERENCES

1. Kameyama M, Kakei M, Sato R, Shibasaki T, Matsuda H, Irisawa H. Intracellular Na+ activates a K+ channel in mammalian cardiac cells. *Nature*. May 24-30 1984;309(5966):354-6. doi:10.1038/309354a0

2. Yuan A, Santi CM, Wei A, et al. The sodium-activated potassium channel is encoded by a member of the Slo gene family. *Neuron*. 2003;37(5):765-773.

3. Joiner WJ, Tang MD, Wang LY, et al. Formation of intermediate-conductance calcium-activated potassium channels by interaction of Slack and Slo subunits. *Nat Neurosci*. Oct 1998;1(6):462-9. doi:10.1038/2176

4. Rizzi S, Knaus HG, Schwarzer C. Differential distribution of the sodium-activated potassium channels slick and slack in mouse brain. *J Comp Neurol*. Jul 1 2016;524(10):2093-116. doi:10.1002/cne.23934

5. Bhattacharjee A, Gan L, Kaczmarek LK. Localization of the Slack potassium channel in the rat central nervous system. *J Comp Neurol*. Dec 16 2002;454(3):241-54. doi:10.1002/cne.10439

6. Yang B, Desai R, Kaczmarek LK. Slack and Slick K(Na) channels regulate the accuracy of timing of auditory neurons. *J Neurosci*. Mar 7 2007;27(10):2617-27. doi:10.1523/JNEUROSCI.5308-06.2007

7. Wallen P, Robertson B, Cangiano L, et al. Sodium-dependent potassium channels

710 of a Slack-like subtype contribute to the slow afterhyperpolarization in lamprey spinal
711 neurons. *J Physiol*. Nov 15 2007;585(Pt 1):75-90. doi:10.1113/jphysiol.2007.138156
712 8. Heron SE, Smith KR, Bahlo M, et al. Missense mutations in the sodium-gated
713 potassium channel gene KCNT1 cause severe autosomal dominant nocturnal frontal
714 lobe epilepsy. *Nat Genet*. Nov 2012;44(11):1188-90. doi:10.1038/ng.2440
715 9. Barcia G, Fleming MR, Deligniere A, et al. De novo gain-of-function KCNT1
716 channel mutations cause malignant migrating partial seizures of infancy. *Nature*
717 *genetics*. 2012;44(11):1255-1259.
718 10. Kingwell K. Mutations in potassium channel KCNT1—a novel driver of epilepsy
719 pathogenesis. *Nature Reviews Neurology*. 2012;8(12):658-658.
720 11. Bonardi CM, Heyne HO, Fiannacca M, et al. KCNT1-related epilepsies and
721 epileptic encephalopathies: phenotypic and mutational spectrum. *Brain*. Dec 31
722 2021;144(12):3635-3650. doi:10.1093/brain/awab219
723 12. McTague A, Nair U, Malhotra S, et al. Clinical and molecular characterization of
724 KCNT1-related severe early-onset epilepsy. *Neurology*. Jan 2 2018;90(1):e55-e66.
725 doi:10.1212/WNL.0000000000004762
726 13. Milligan CJ, Li M, Gazina EV, et al. KCNT1 gain of function in 2 epilepsy
727 phenotypes is reversed by quinidine. *Annals of neurology*. 2014;75(4):581-590.
728 14. Bearden D, Strong A, Ehnot J, DiGiovine M, Dlugos D, Goldberg EM. Targeted
729 treatment of migrating partial seizures of infancy with quinidine. *Ann Neurol*. Sep
730 2014;76(3):457-61. doi:10.1002/ana.24229

731 15. Mikati MA, Jiang YH, Carboni M, et al. Quinidine in the treatment of KCNT1-
732 positive epilepsies. *Ann Neurol*. Dec 2015;78(6):995-9. doi:10.1002/ana.24520
733 16. Numis AL, Nair U, Datta AN, et al. Lack of response to quinidine in KCNT 1-
734 related neonatal epilepsy. *Epilepsia*. 2018;59(10):1889-1898.
735 17. Liu R, Sun L, Wang Y, Wang Q, Wu J. New use for an old drug: quinidine in
736 KCNT1-related epilepsy therapy. *Neurol Sci*. Nov 28 2022;doi:10.1007/s10072-022-
737 06521-x
738 18. Cole BA, Clapcote SJ, Muench SP, Lippiat JD. Targeting KNa1.1 channels in
739 KCNT1-associated epilepsy. *Trends Pharmacol Sci*. Aug 2021;42(8):700-713.
740 doi:10.1016/j.tips.2021.05.003
741 19. Xu D, Chen S, Yang J, Wang X, Fang Z, Li M. Precision therapy with quinidine of
742 KCNT1-related epileptic disorders: A systematic review. *Br J Clin Pharmacol*. Dec
743 2022;88(12):5096-5112. doi:10.1111/bcp.15479
744 20. Zhang Z, Rosenhouse-Dantsker A, Tang QY, Noskov S, Logothetis DE. The RCK2
745 domain uses a coordination site present in Kir channels to confer sodium sensitivity to
746 Slo2.2 channels. *J Neurosci*. Jun 2 2010;30(22):7554-62.
747 doi:10.1523/JNEUROSCI.0525-10.2010
748 21. Budelli G, Hage TA, Wei A, et al. Na+-activated K+ channels express a large
749 delayed outward current in neurons during normal physiology. *Nat Neurosci*. Jun
750 2009;12(6):745-50. doi:10.1038/nn.2313
751 22. Hage TA, Salkoff L. Sodium-activated potassium channels are functionally

752 coupled to persistent sodium currents. *J Neurosci*. Feb 22 2012;32(8):2714-21.
753 doi:10.1523/JNEUROSCI.5088-11.2012
754 23. Nanou E, Kyriakatos A, Bhattacharjee A, Kaczmarek LK, Paratcha G, El Manira
755 A. Na+-mediated coupling between AMPA receptors and KNa channels shapes synaptic
756 transmission. *Proceedings of the National Academy of Sciences*. 2008;105(52):20941-
757 20946.
758 24. Goldin AL. Resurgence of sodium channel research. *Annu Rev Physiol*.
759 2001;63:871-94. doi:10.1146/annurev.physiol.63.1.871
760 25. Trimmer JS, Rhodes KJ. Localization of voltage-gated ion channels in mammalian
761 brain. *Annu Rev Physiol*. 2004;66:477-519.
762 doi:10.1146/annurev.physiol.66.032102.113328
763 26. Lai HC, Jan LY. The distribution and targeting of neuronal voltage-gated ion
764 channels. *Nat Rev Neurosci*. Jul 2006;7(7):548-62. doi:10.1038/nrn1938
765 27. Pickard L, Noel J, Henley JM, Collingridge GL, Molnar E. Developmental changes
766 in synaptic AMPA and NMDA receptor distribution and AMPA receptor subunit
767 composition in living hippocampal neurons. *J Neurosci*. Nov 1 2000;20(21):7922-31.
768 28. Cole BA, Johnson RM, Dejakaisaya H, et al. Structure-Based Identification and
769 Characterization of Inhibitors of the Epilepsy-Associated KNa1.1 (KCNT1) Potassium
770 Channel. *iScience*. May 22 2020;23(5):101100. doi:10.1016/j.isci.2020.101100
771 29. Kaczmarek LK. Slack, Slick and Sodium-Activated Potassium Channels. *ISRN*
772 *Neurosci*. Apr 18 2013;2013(2013)doi:10.1155/2013/354262

773 30. Bhattacharjee A, Joiner WJ, Wu M, Yang Y, Sigworth FJ, Kaczmarek LK. Slick
774 (Slo2.1), a rapidly-gating sodium-activated potassium channel inhibited by ATP. *J*
775 *Neurosci*. Dec 17 2003;23(37):11681-91.
776 31. Rosker C, Lohberger B, Hofer D, Steinecker B, Quasthoff S, Schreibmayer W. The
777 TTX metabolite 4, 9-anhydro-TTX is a highly specific blocker of the Nav1. 6 voltage-
778 dependent sodium channel. *American Journal of Physiology-Cell Physiology*.
779 2007;293(2):C783-C789.
780 32. Rush AM, Dib-Hajj SD, Waxman SG. Electrophysiological properties of two
781 axonal sodium channels, Nav1.2 and Nav1.6, expressed in mouse spinal sensory
782 neurones. *J Physiol*. May 1 2005;564(Pt 3):803-15. doi:10.1113/jphysiol.2005.083089
783 33. Chatelier A, Zhao J, Bois P, Chahine M. Biophysical characterisation of the
784 persistent sodium current of the Nav1.6 neuronal sodium channel: a single-channel
785 analysis. *Pflugers Arch*. Jun 2010;460(1):77-86. doi:10.1007/s00424-010-0801-9
786 34. Urbani A, Belluzzi O. Riluzole inhibits the persistent sodium current in mammalian
787 CNS neurons. *Eur J Neurosci*. Oct 2000;12(10):3567-74. doi:10.1046/j.1460-
788 9568.2000.00242.x
789 35. Lukacs P, Foldi MC, Valanszki L, et al. Non-blocking modulation contributes to
790 sodium channel inhibition by a covalently attached photoreactive riluzole analog. *Sci*
791 *Rep*. May 25 2018;8(1):8110. doi:10.1038/s41598-018-26444-y
792 36. Hu W, Tian C, Li T, Yang M, Hou H, Shu Y. Distinct contributions of Na(v)1.6 and
793 Na(v)1.2 in action potential initiation and backpropagation. *Nat Neurosci*. Aug

794 2009;12(8):996-1002. doi:10.1038/nn.2359

795 37. Liu Y, Lai S, Ma W, et al. CDYL suppresses epileptogenesis in mice through
796 repression of axonal Nav1.6 sodium channel expression. *Nat Commun*. Aug 25
797 2017;8(1):355. doi:10.1038/s41467-017-00368-z

798 38. Takanishi CL, Bykova EA, Cheng W, Zheng J. GFP-based FRET analysis in live
799 cells. *Brain Res*. May 26 2006;1091(1):132-9. doi:10.1016/j.brainres.2006.01.119

800 39. Dilena R, DiFrancesco JC, Soldovieri MV, et al. Early Treatment with Quinidine
801 in 2 Patients with Epilepsy of Infancy with Migrating Focal Seizures (EIMFS) Due to
802 Gain-of-Function KCNT1 Mutations: Functional Studies, Clinical Responses, and
803 Critical Issues for Personalized Therapy. *Neurotherapeutics*. Oct 2018;15(4):1112-1126.
804 doi:10.1007/s13311-018-0657-9

805 40. Abdelnour E, Gallentine W, McDonald M, Sachdev M, Jiang Y-H, Mikati MA.
806 Does age affect response to quinidine in patients with KCNT1 mutations? Report of
807 three new cases and review of the literature. *Seizure*. 2018;55:1-3.

808 41. Rizzo F, Ambrosino P, Guacci A, et al. Characterization of two de novoKCNT1
809 mutations in children with malignant migrating partial seizures in infancy. *Mol Cell*
810 *Neurosci*. Apr 2016;72:54-63. doi:10.1016/j.mcn.2016.01.004

811 42. Barcia G, Chemaly N, Kuchenbuch M, et al. Epilepsy with migrating focal seizures:
812 KCNT1 mutation hotspots and phenotype variability. *Neurol Genet*. Dec
813 2019;5(6):e363. doi:10.1212/NXG.0000000000000363

814 43. Nadler JV. Kainic acid as a tool for the study of temporal lobe epilepsy. *Life*

815 *sciences*. 1981;29(20):2031-2042.

816 44. Levesque M, Avoli M. The kainic acid model of temporal lobe epilepsy. *Neurosci*

817 *Biobehav R*. Dec 2013;37(10):2887-2899. doi:10.1016/j.neubiorev.2013.10.011

818 45. Pinel JP, Rovner LI. Electrode placement and kindling-induced experimental

819 epilepsy. *Exp Neurol*. Jan 15 1978;58(2):335-46. doi:10.1016/0014-4886(78)90145-0

820 46. Kim EC, Zhang J, Tang AY, et al. Spontaneous seizure and memory loss in mice

821 expressing an epileptic encephalopathy variant in the calmodulin-binding domain of

822 Kv7.2. *Proc Natl Acad Sci U S A*. Dec 21 2021;118(51)doi:10.1073/pnas.2021265118

823 47. Ehinger R, Kuret A, Matt L, et al. Slack K(+) channels attenuate NMDA-induced

824 excitotoxic brain damage and neuronal cell death. *FASEB J.* May 2021;35(5):e21568.

825 doi:10.1096/fj.202002308RR

826 48. Markham MR, Kaczmarek LK, Zakon HH. A sodium-activated potassium channel

827 supports high-frequency firing and reduces energetic costs during rapid modulations of

828 action potential amplitude. *J Neurophysiol*. Apr 2013;109(7):1713-23.

829 doi:10.1152/jn.00875.2012

830 49. Kole MH, Ilschner SU, Kampa BM, Williams SR, Ruben PC, Stuart GJ. Action

831 potential generation requires a high sodium channel density in the axon initial segment.

832 *Nat Neurosci*. Feb 2008;11(2):178-86. doi:10.1038/nn2040

833 50. Lazarov E, Dannemeyer M, Feulner B, et al. An axon initial segment is required

834 for temporal precision in action potential encoding by neuronal populations. *Science*

835 *advances*. 2018;4(11):eaau8621.

836 51. Katz E, Stoler O, Scheller A, et al. Role of sodium channel subtype in action
837 potential generation by neocortical pyramidal neurons. *Proc Natl Acad Sci U S A*. Jul
838 24 2018;115(30):E7184-E7192. doi:10.1073/pnas.1720493115
839 52. Brown MR, Kronengold J, Gazula VR, et al. Amino-termini isoforms of the Slack
840 K+ channel, regulated by alternative promoters, differentially modulate rhythmic firing
841 and adaptation. *J Physiol*. Nov 1 2008;586(21):5161-79.
842 doi:10.1113/jphysiol.2008.160861
843 53. Hite RK, MacKinnon R. Structural Titration of Slo2.2, a Na(+)-Dependent K(+)
844 Channel. *Cell*. Jan 26 2017;168(3):390-399 e11. doi:10.1016/j.cell.2016.12.030
845 54. Gertler T, Bearden D, Bhattacharjee A, Carvill G. KCNT1-Related Epilepsy. In:
846 Adam MP, Ardinger HH, Pagon RA, et al, eds. *GeneReviews((R))*. 1993.
847 55. Fitzgerald MP, Fiannacca M, Smith DM, et al. Treatment Responsiveness in
848 KCNT1-Related Epilepsy. *Neurotherapeutics*. Jul 2019;16(3):848-857.
849 doi:10.1007/s13311-019-00739-y
850 56. Griffin AM, Kahlig KM, Hatch RJ, et al. Discovery of the First Orally Available,
851 Selective KNa1.1 Inhibitor: In Vitro and In Vivo Activity of an Oxadiazole Series. *ACS*
852 *Med Chem Lett*. Apr 8 2021;12(4):593-602. doi:10.1021/acsmedchemlett.0c00675
853 57. Spitznagel BD, Mishra NM, Qunies AM, et al. VU0606170, a Selective Slack
854 Channels Inhibitor, Decreases Calcium Oscillations in Cultured Cortical Neurons. *ACS*
855 *Chem Neurosci*. Nov 4 2020;11(21):3658-3671. doi:10.1021/acschemneuro.0c00583
856 58. Tang QY, Zhang FF, Xu J, et al. Epilepsy-Related Slack Channel Mutants Lead to

857 Channel Over-Activity by Two Different Mechanisms. *Cell Rep*. Jan 5 2016;14(1):129-
858 139. doi:10.1016/j.celrep.2015.12.019
859 59. Qiu S, Hua YL, Yang F, Chen YZ, Luo JH. Subunit assembly of N-methyl-d-
860 aspartate receptors analyzed by fluorescence resonance energy transfer. *J Biol Chem*.
861 Jul 1 2005;280(26):24923-30. doi:10.1074/jbc.M413915200
862 60. Cheng W, Yang F, Takanishi CL, Zheng J. Thermosensitive TRPV channel subunits
863 coassemble into heteromeric channels with intermediate conductance and gating
864 properties. *Journal of General Physiology*. 2007;129(3):191-207.
865 61. Zou L, Peng Q, Wang P, Zhou B. Progress in Research and Application of HIV-1
866 TAT-Derived Cell-Penetrating Peptide. *J Membr Biol*. Apr 2017;250(2):115-122.
867 doi:10.1007/s00232-016-9940-z
868 62. Zheng J, Trudeau MC, Zagotta WN. Rod cyclic nucleotide-gated channels have a
869 stoichiometry of three CNGA1 subunits and one CNGB1 subunit. *Neuron*.
870 2002;36(5):891-896.
871 63. Yang F, Cui Y, Wang K, Zheng J. Thermosensitive TRP channel pore turret is part
872 of the temperature activation pathway. *Proceedings of the National Academy of*
873 *Sciences*. 2010;107(15):7083-7088.
874 64. Erickson MG, Alseikhan BA, Peterson BZ, Yue DT. Preassociation of calmodulin
875 with voltage-gated Ca2+ channels revealed by FRET in single living cells. *Neuron*.
876 2001;31(6):973-985.
877 65. Chai AP, Chen XF, Xu XS, et al. A Temporal Activity of CA1 Neurons Underlying

878 Short-Term Memory for Social Recognition Altered in PTEN Mouse Models of Autism
879 Spectrum Disorder. *Front Cell Neurosci*. 2021;15:699315.
880 doi:10.3389/fncel.2021.699315
881 66. Huang Z, Walker MC, Shah MM. Loss of dendritic HCN1 subunits enhances
882 cortical excitability and epileptogenesis. *J Neurosci*. Sep 2 2009;29(35):10979-88.
883 doi:10.1523/JNEUROSCI.1531-09.2009
884 67. He X-P, Kotloski R, Nef S, Luikart BW, Parada LF, McNamara JO. Conditional
885 deletion of TrkB but not BDNF prevents epileptogenesis in the kindling model. *Neuron*.
886 2004;43(1):31-42.
887 68. Racine RJ. Modification of seizure activity by electrical stimulation. II. Motor
888 seizure. *Electroencephalogr Clin Neurophysiol*. Mar 1972;32(3):281-94.
889 doi:10.1016/0013-4694(72)90177-0
890 69. Huang Z, Lujan R, Martinez-Hernandez J, Lewis AS, Chetkovich DM, Shah MM.
891 TRIP8b-independent trafficking and plasticity of adult cortical presynaptic HCN1
892 channels. *J Neurosci*. Oct 17 2012;32(42):14835-48. doi:10.1523/JNEUROSCI.1544-
893 12.2012
894

895

Main Figures for

Coupling of Slack and Nav1.6 sensitizes Slack to quinidine blockade and guides anti-seizure strategy development

Tian Yuan *et al.*

*Corresponding author. Email: huangz@hsc.pku.edu.cn

This PDF file includes:

Figure. 1 to 7

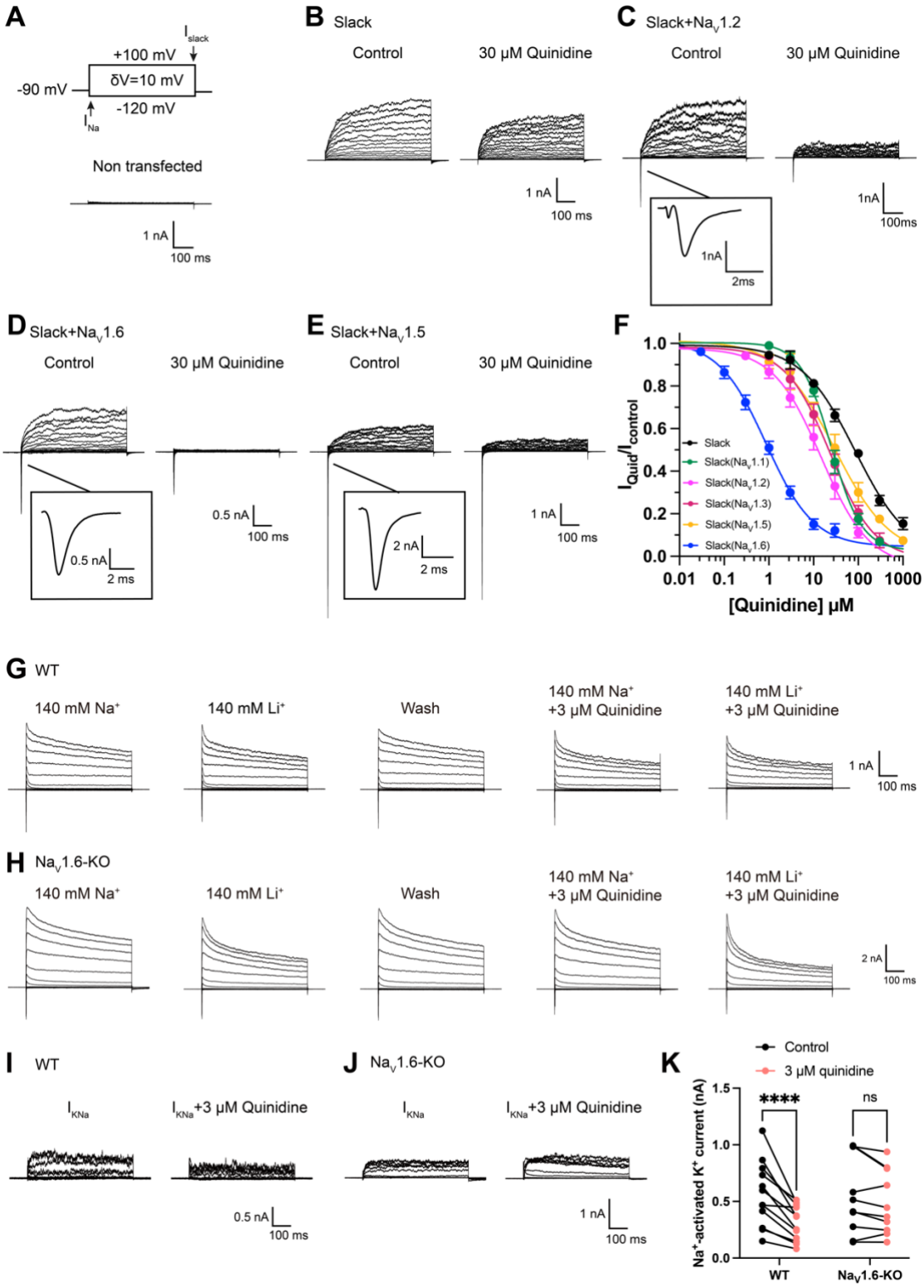

Figure 1. **Nav1.6 specifically sensitizes Slack to quinidine blockade.** (**A**) The voltage protocol and current traces from control (non-transfected) HEK293 cells. The arrows on the voltage protocol indicate the onset of inward sodium currents through Nav channels and delayed outward potassium currents through Slack channels. The currents

were evoked by applying 600-ms step pulses to voltages varying from -120 mV to +100 mV in 10 mV increments, with a holding potential of -90 mV and a stimulus frequency of 0.20 Hz. (**B**) Example current traces from HEK293 cells expressing Slack alone. The left traces show the family of control currents; the right traces show Slack currents remaining after application of 1 μM quinidine in the bath solution. (**C-E**) Example current traces from HEK293 cells co-expressing Slack with $Na_V1.2$ (**C**), $Na_V1.6$ (**D**), or $Na_V1.5$ (**E**) channels before and after application of 30 μM quinidine. (**F**) The concentration-response curves for blocking of Slack by quinidine at +100 mV upon expression of Slack alone (n = 6) and co-expression of Slack with $Na_V1.1$ (n = 7), $Na_V1.2$ (n = 10), $Na_V1.3$ (n = 13), $Na_V1.5$ (n = 9), or $Na_V1.6$ (n = 19). Please refer to Supplementary Table 1 for IC_{50} values. (**G-H**) Delayed outward currents in primary cortical neurons from $Na_V1.6$ knockout C3HeB/FeJ mice ($Na_V1.6$-KO) (**H**) and the wild-type littermate controls (WT) (**G**). Current traces were elicited by 600-ms step pulses to voltages varying from -120 mV to +100 mV in 20 mV increments, with a holding potential of -70 mV, and recorded with different bath solutions in the following order: Na^+-based bath solution ($I_{Control}$), replacement of external Na^+ with Li^+ in equivalent concentration (I_{Li}), washout of quinidine by Na^+-based bath solution (I_{Wash}), Na^+-based bath solution with 3 μM quinidine (I_{Quid}), Li^+-based bath solution with 3 μM quinidine ($I_{Li+Quid}$). The removal and subsequent replacement of extracellular Na^+ revealed the I_{KNa} in neurons. (**I-J**), The sensitivity of native sodium-activated potassium currents (I_{KNa}) to 3 μM quinidine blockade in WT (**I**) and $Na_V1.6$-KO (**J**) neurons. I_{KNa} before application of quinidine was obtained from the subtraction of $I_{Control}$ and I_{Li}. Maintained I_{KNa} after application of 3 μM quinidine was obtained from the subtraction of I_{Quid} and $I_{Li+Quid}$. (**K**) Summarized amplitudes of I_{KNa} before and after application of 3 μM quinidine in the bath solution in WT (black, n = 12) and $Na_V1.6$-KO (red, n = 10)

primary cortical neurons. ****$p < 0.0001$, Two-way repeated measures ANOVA followed by Bonferroni's post hoc test.

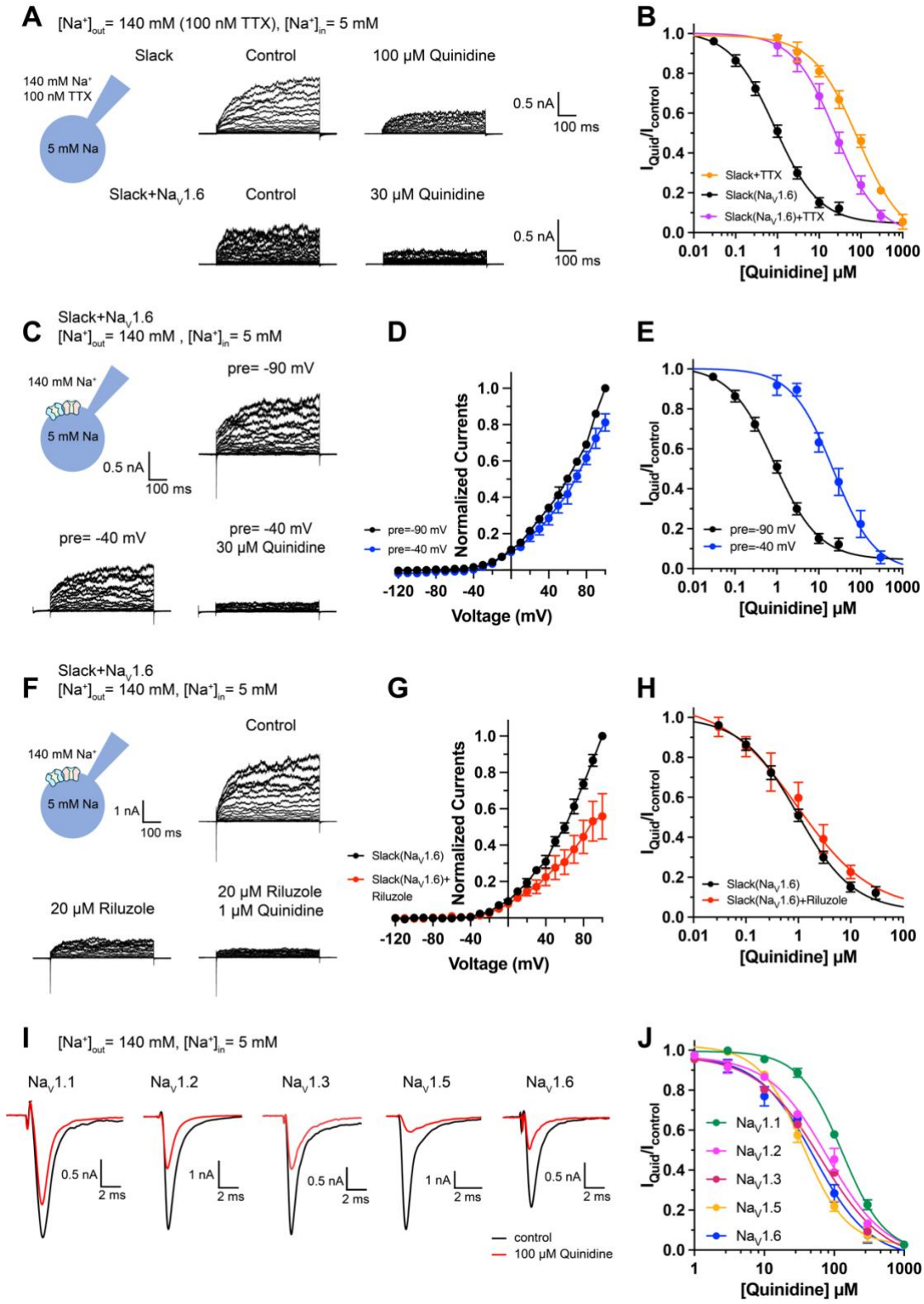

Figure 2. Blocking transient sodium influx through Nav1.6 reduces Nav1.6-mediated sensitization of Slack to quinidine blockade. (**A**) Example current traces from HEK293 cells expressing Slack alone (top) and co-expressing Slack with Nav1.6

(bottom), with 100nM TTX in the bath solution. The left traces show the family of control currents; the right traces show Slack currents remaining after application of quinidine. (**B**) The concentration-response curves for blocking of Slack by quinidine upon expression of Slack alone (n = 3) and co-expression of Slack with $Na_V1.6$ (n = 7), with 100 nM TTX in the bath solution. (**C**) Top, example current traces recorded from a HEK293 cell co-expressing Slack with $Na_V1.6$ and evoked from a 100-ms prepulse (pre) of -90 mV. Bottom, example current traces recorded from the same cell but evoked from a 100-ms prepulse of -40 mV, before and after application of quinidine. (**D**) I-V curves of Slack upon co-expression with $Na_V1.6$. The currents were evoked from a prepulse of -90 mV (black) or -40 mV (blue). (**E**) The concentration-response curves for blocking of Slack by quinidine with a prepulse of -90 mV (black, n = 19) or -40 mV (blue, n = 5). (**F**) Top, example current traces recorded from a HEK293 cell co-expressing Slack and $Na_V1.6$ without riluzole in the bath solution. Bottom, example current traces recorded from the same cell with 20 μM riluzole in the bath solution, before and after application of quinidine. (**G**) I-V curves of Slack upon co-expression with $Na_V1.6$ before (black) and after (red) application of 20 μM riluzole into bath solution.The concentration-response curves for blocking of Slack by quinidine upon co-expression of Slack with $Na_V1.6$, without (n = 19) or with (n = 6) 20 μM riluzole in the bath solution. (**I-J**) The sensitivity of Na_V channel subtypes to quinidine blockade upon expression of Na_V alone in HEK293 cells. Example current traces (**I**) were evoked by a 50-ms step depolarization to 0 mV from a holding potential of -90 mV. The Concentration-response curves for blocking of Na_V channel subtypes by quinidine (**J**) were shown on the right panel (n = 5 for $Na_V1.1$, n = 3 for $Na_V1.2$, n = 6 for $Na_V1.3$, n = 6 for $Na_V1.5$, and n = 4 for $Na_V1.6$).

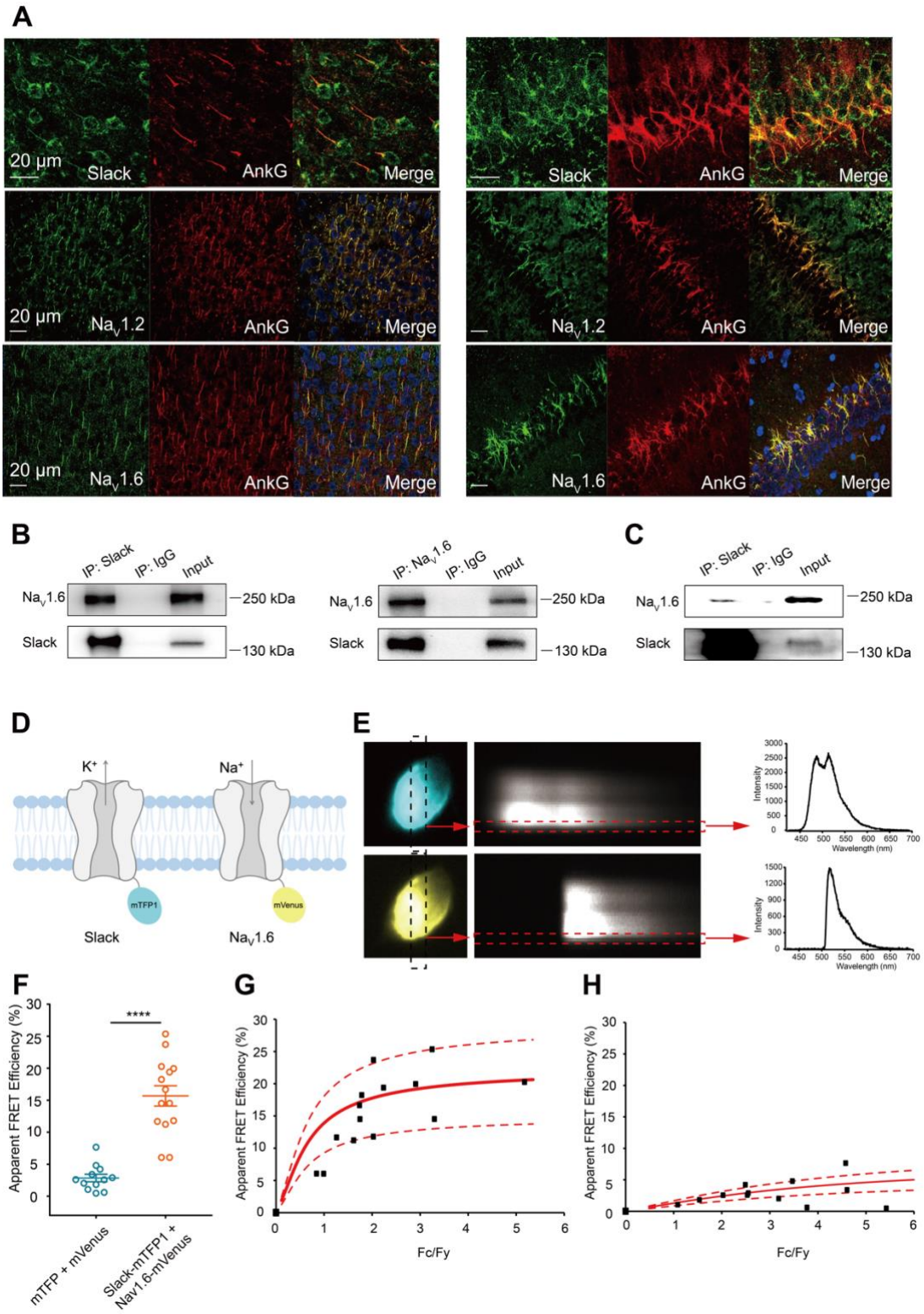

Figure 3. Slack physically interacts with Nav1.6 *in vitro* and *in vivo*. (**A**) Immunofluorescence of Slack, Nav1.2, Nav1.6 (green), and AnkG (red) in hippocampus CA1 (left) and neocortex (right). Confocal microscopy images were obtained from Coronary brain slices of C57BL/6 mice. (**B**) Coimmunoprecipitation

(Co-IP) of Slack and Nav1.6 in cell lysates from HEK293T cells co-transfected with Slack and Nav1.6. (**C**) Co-IP of Slack and Nav1.6 in mouse brain tissue lysates. Input volume corresponds to 10% of the total lysates for Co-IP. (**D**) A schematic diagram showing the fluorescence-labeled Slack and Nav1.6. mTFP1 and mVenus were fused to the C-terminal region of Slack (Slack-mTFP1) and Nav1.6 (Nav1.6-mVenus), respectively. (**E**) FRET imaging of Slack-mTFP1 and Nav1.6-mVenus co-expressed in HEK293 cells. The emission spectra measured from the edge of cell (dotted arrows in red) are used for FRET efficiency calculation. (**F**) The apparent FRET efficiency measured from cells co-expressing the fluorophore-tagged ion channels or co-expressing the fluorophores. **** $p < 0.0001$, unpaired two-tailed Student's *t* test. (**G-H**) The FRET efficiency measured from cells co-expressing the fluorophore-tagged ion channels (**G**), or from cells co-expressing fluorophores (**H**). The efficiency value was plotted as a function of the fluorescence intensity ratio between mTFP1 and mVenus (Fc/Fy). Each symbol represents a single cell. The solid curve represents the FRET model that yields the best fit; dotted curves represent models with 5% higher or lower FRET efficiencies.

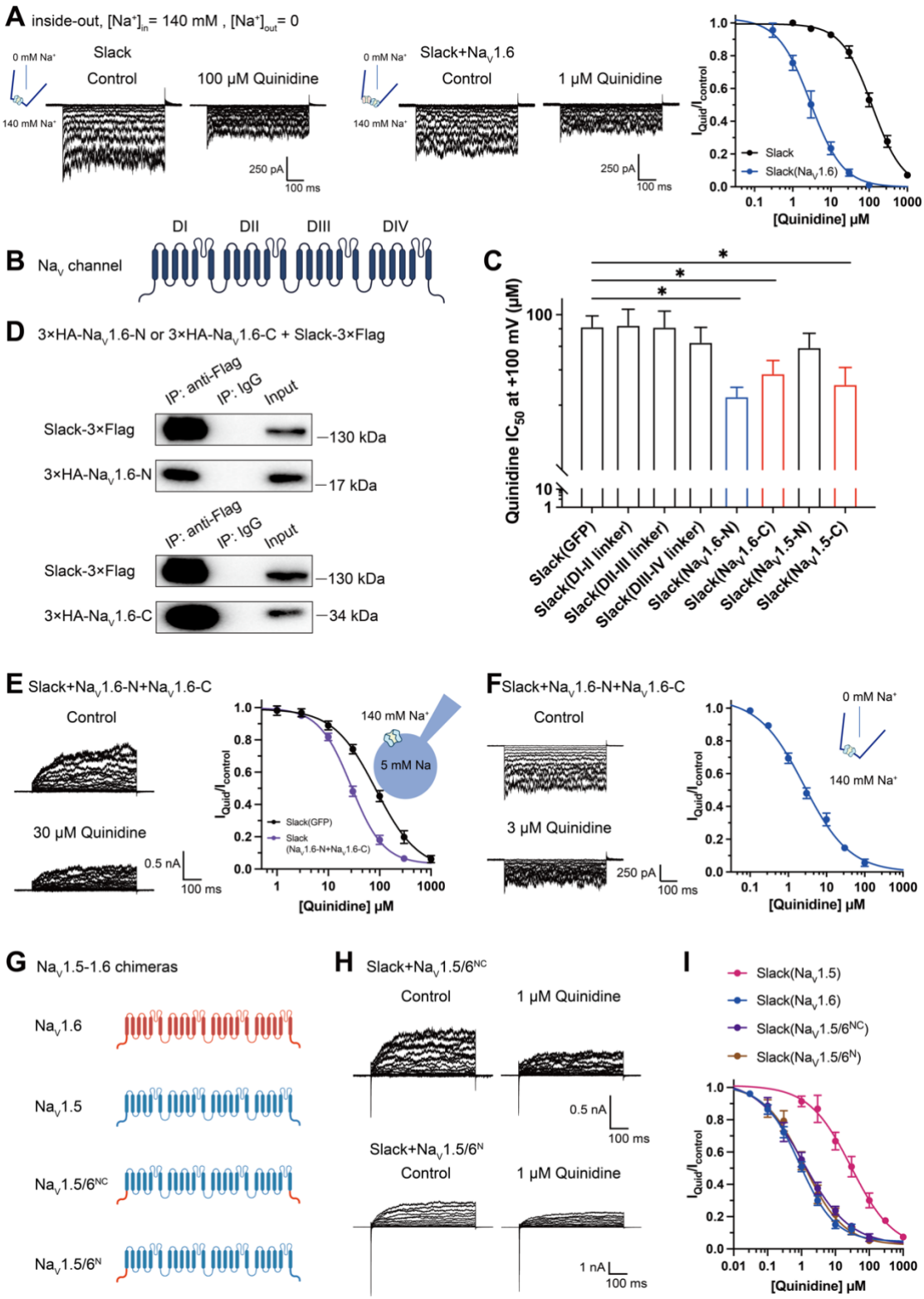

Figure 4. Nav1.6's N- and C-termini interacting with Slack is a prerequisite for Nav1.6-mediated sensitization of Slack to quinidine blockade. (**A**) The sensitivity of Slack to quinidine blockade upon expression of Slack alone (n = 3) and co-expression

of Slack with $Na_V1.6$ (n = 3) from excised inside-out patches. The pipette solution contained (in mM) 130 KCl, 1 EDTA, 10 HEPES and 2 $MgCl_2$ (pH 7.3); the bath solution contained (in mM) 140 NaCl, 1 EDTA, 10 HEPES and 2 $MgCl_2$ (pH 7.4). The membrane voltage was held at 0 mV and stepped to voltages varying from −100 mV to 0 mV in 10 mV increments. Example current traces were shown on the left panel. The concentration-response curves for blocking of Slack by quinidine were shown on the right panel. (**B**) Domain architecture of the human Na_V channel pore-forming α subunit. (**C**) Calculated IC_{50} values at +100 mV of quinidine on Slack upon co-expression with indicated cytoplasmic fragments from Na_V channels. For $Na_V1.6$, cytoplasmic fragments used include N-terminus ($Na_V1.6$-N, residues 1-132), inter domain linkers (Domain I-II linker, residues 409-753; Domain II-III linker, residues 977-1199; Domain III-IV linker, residues 1461-1523), and C-terminus ($Na_V1.6$-C, residues 1766-1980). For $Na_V1.5$, cytoplasmic fragments used include N-terminus ($Na_V1.5$-N, residues 1-131) and C-terminus ($Na_V1.5$-C, residues 1772-2016). (**D**) Co-IP of Slack and terminal domains of $Na_V1.6$ in cell lysates from HEK293T cells co-expressing 3×Flag-tagged Slack (Slack-3×Flag) and 3×HA-tagged termini of $Na_V1.6$ (3×HA-$Na_V1.6$-N or 3×HA-$Na_V1.6$-C). The 3×Flag tag was fused to the C-terminal region of Slack and the 3×HA tag was fused to the N-terminal region of $Na_V1.6$'s fragments. (**E**) The sensitivity of Slack to quinidine blockade upon co-expression of Slack with GFP (n = 12) or N- and C-termini of $Na_V1.6$ (n = 11), from whole-cell recordings. (**F**) The sensitivity of Slack to quinidine blockade upon co-expression of Slack with N- and C-termini of $Na_V1.6$, from excised inside-out recordings (n = 10, using the same protocols as in Fig. 4A). Example current traces before and after application of quinidine were shown on the left panel. The concentration-response curves were shown on the right panel. (**G**) A schematic diagram of the $Na_V1.5$-1.6 chimeric channels ($Na_V1.5/6^{NC}$ and

Nav1.5/6^{N}) used in this study. (**H**) Example current traces recorded from HEK293 cells co-expressing Slack and Nav1.5-1.6 chimeras before and after application of the indicated concentration of quinidine. (**I**) The concentration-response curves for blocking of Slack by quinidine upon co-expression of Slack with Nav1.5 (n = 9), Nav1.6 (n = 19), Nav1.5/6^{NC} (n = 9), or Nav1.5/6^{N} (n = 9).

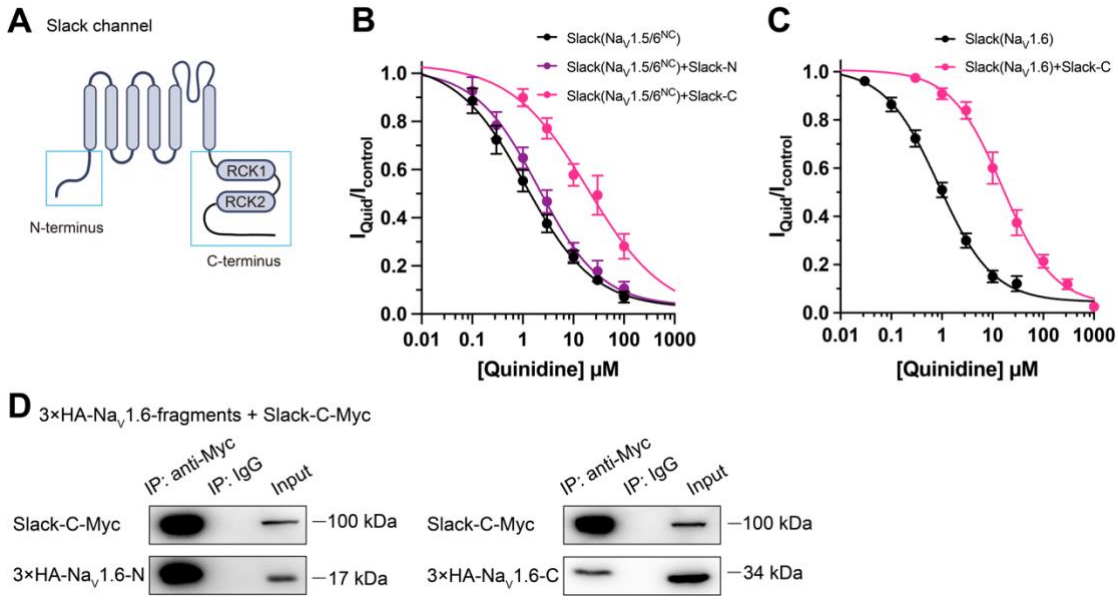

Figure 5. Slack's C-terminus is required for Nav1.6-mediated sensitization of Slack to quinidine blockade. (**A**) Domain architecture of the human Slack channel subunit. Slack's N-terminus (Slack-N, residues 1-116) and C-terminus (Slack-C, residues 345-1235) were shown in the blue boxes. (**B**) The concentration-response curves for blocking of Slack by quinidine upon additional expression of Slack's N- or C-terminus in HEK293T cells co-expressing Slack and Nav1.5/6^{NC}. (**C**) The concentration-response curves for blocking Slack by quinidine upon additional expression of Slack's C-terminus in HEK293 cells co-expressing Slack and Nav1.6. (**D**) Co-IP of Myc-tagged Slack's C-terminus (Slack-C-Myc) with 3×HA-tagged Nav1.6's termini (3×HA-Nav1.6-N or 3×HA-Nav1.6-C) in HEK293T cell lysates. The 3×HA tag was fused to the N-terminal region of Nav1.6's fragments, and the Myc tag was fused to the C-terminal region of Slack's fragment.

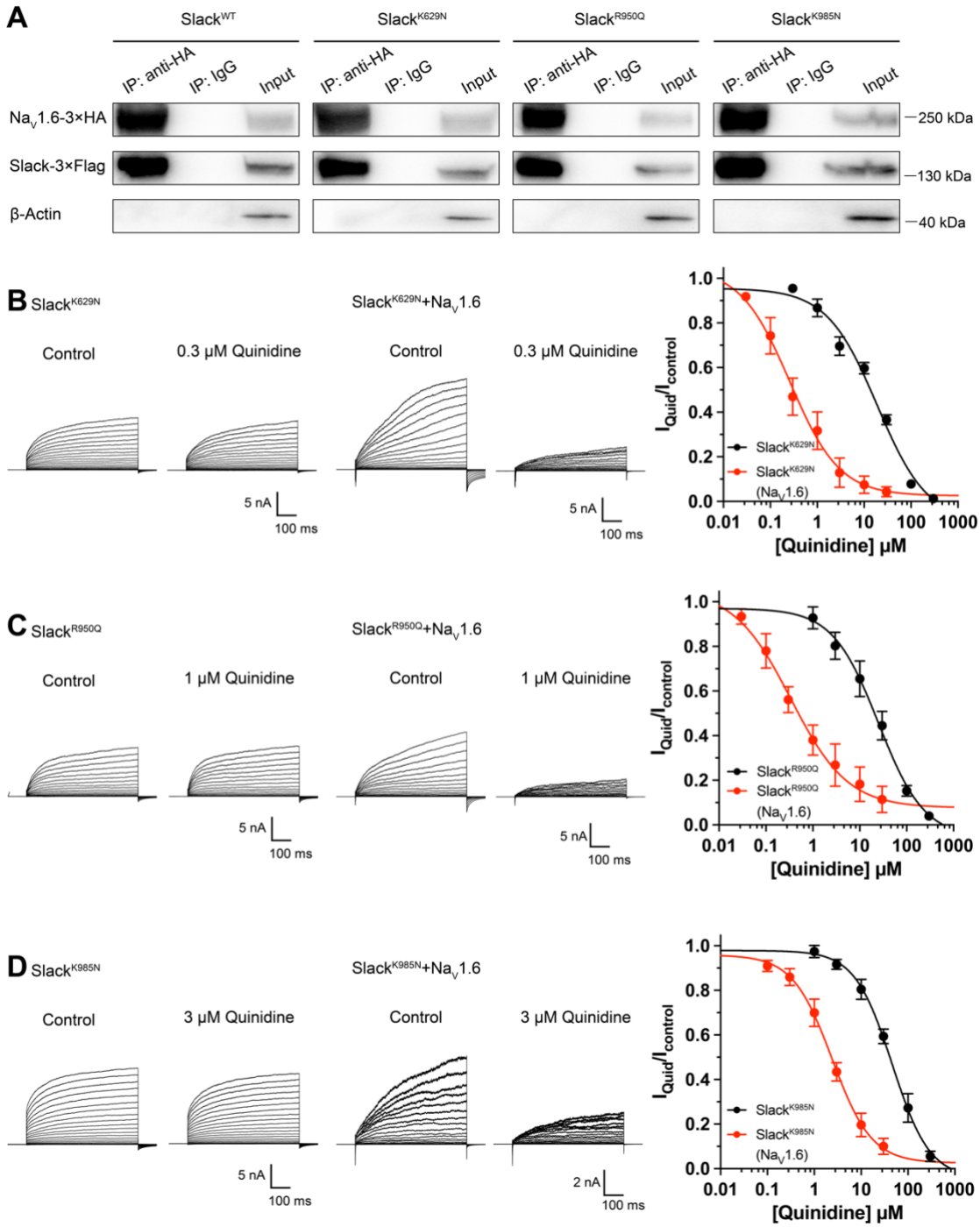

Figure 6. Nav1.6 sensitizes epilepsy-related Slack mutant variants to quinidine blockade. (**A**) Co-IP of 3×Flag-tagged Slack or its mutations (Slack-3×Flag) with 3×HA-tagged Nav1.6 (Nav1.6-3×HA) in HEK293T cell lysates. The tags were all fused to the C-terminal region of wild-type or mutant ion channels. (**B-D**) The sensitivity of Slack mutant variants (Slack^{K629N} [**B**], Slack^{R950Q} [**C**], and Slack^{K985N} [**D**]) to quinidine blockade upon expression of Slack mutant variants alone and co-expression of Slack

mutant variants with $Na_V1.6$. Left, example current traces recorded from HEK293 cells expressing Slack mutant variants alone and co-expressing Slack mutant variants with $Na_V1.6$, before and after application of the indicated concentrations of quinidine. Right, the concentration-response curves for blocking of Slack mutant variants by quinidine upon expression of Slack mutant variants alone (n = 8 for $Slack^{K629N}$, n = 7 for $Slack^{R950Q}$, and n = 5 for $Slack^{K985N}$) and co-expression of Slack mutant variants with $Na_V1.6$ (n = 8 for $Slack^{K629N}$ upon co-expression with $Na_V1.6$, n = 5 for $Slack^{R950Q}$ upon co-expression with $Na_V1.6$, and n = 7 for $Slack^{K985N}$ upon co-expression with $Na_V1.6$). Please refer to Supplementary Table 4 for IC_{50} values.

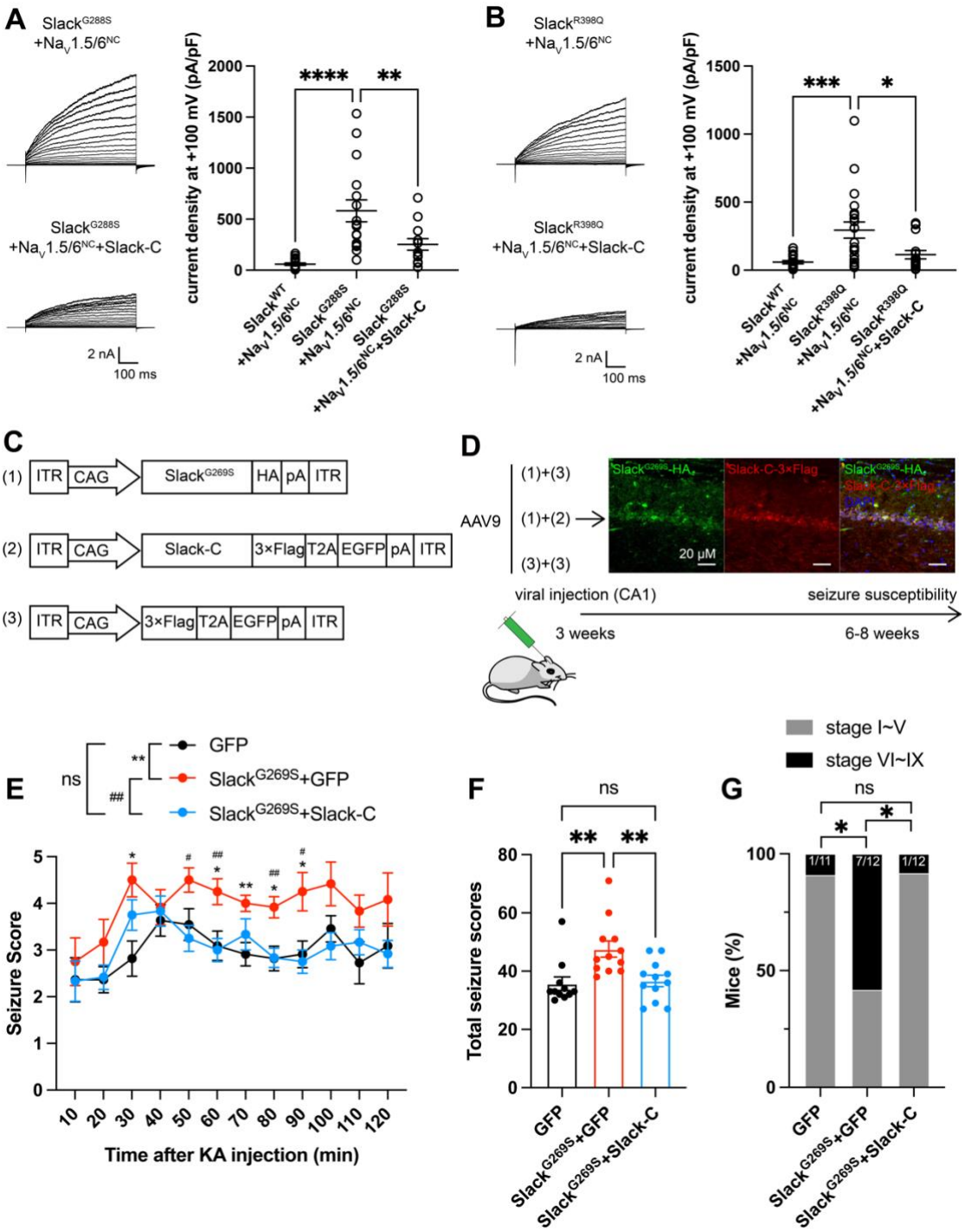

Figure 7. Viral expression of Slack's C-terminus prevents Slack^{G269S}-induced seizures. (**A-B**) The current densities of Slack mutant variants (Slack^{G288S} [**A**] and Slack^{R398Q} [**B**]) upon co-expression with Nav1.5/6^{NC} in HEK293T cells were reduced by additional expression of Slack's C-terminus. Left, example current traces from HEK293T cells co-expressing Slack mutant variants and Nav1.5/6^{NC} or co-expressing

Slack mutant variants, $Nav1.5/6^{NC}$, and Slack's C-terminus. Right, summarized current densities at +100 mV. * $p < 0.05$, ** $p < 0.01$, *** $p < 0.001$; one-way ANOVA followed by Bonferroni's post hoc test. (**C**) Architecture for expression cassettes of AAVs. (**D**) Top, Immunofluorescence of HA-tagged $Slack^{G269S}$ (green), 3×Flag-tagged Slack's C-terminus (red), and DAPI (blue) at 5 weeks after viral injection of $Slack^{G269S}$ with Slack's C-terminus into CA1 of mice. Bottom, study design and timeline for the stereotactic injection model. (**E**) Time-course of KA-induced seizure stage changes at 10-min intervals based on a modified Racine, Pinal, and Rovner scale (please refer to Methods for further details). The number of mice used: "GFP" control group (n = 11), "$Slack^{G269S}$+GFP" group (n = 12), "$Slack^{G269S}$+Slack-C" group (n = 12). "GFP" vs. "$Slack^{G269S}$+GFP": $F_{(1,21)} = 10.48$, $p = 0.0040$, * $p < 0.05$, ** $p < 0.01$; "$Slack^{G269S}$+GFP" vs. "$Slack^{G269S}$+Slack-C": $F_{(1,22)} = 10.30$, $p = 0.0040$, $^{\#}$ $p < 0.05$, $^{\#\#}$ $p < 0.01$. "GFP" vs. "$Slack^{G269S}$+Slack-C": $F_{(1,21)} = 0.09574$, $p = 0.7600$. Repeated two-way ANOVA followed by Bonferroni's post hoc test. (**F**) Total seizure score per mouse over the 2 h after KA injection of these three groups. * $p < 0.05$, ** $p < 0.01$; one-way ANOVA followed by Bonferroni's post hoc test. (**G**) The percentage of mice with stage VI~IX seizures over the 2 h after KA injection in each group. * $p < 0.05$; Fisher's exact test.